An important role for Myb-MuvB and its target gene KIF23 in a mouse model of lung adenocarcinoma

Fabian Iltzsche[1*], Katja Simon[1*], Sabine Stopp[1*], Grit Pattschull[1*], Sven Francke[1], Patrick Wolter[1], Stefanie Hauser[1], Daniel J. Murphy[4], Paloma Garcia[5], Andreas Rosenwald[2,3] and Stefan Gaubatz[1,2,6]

[1]Theodor Boveri Institute, Biocenter, University of Wuerzburg and [2]Comprehensive Cancer Center Mainfranken, University of Wuerzburg, and [3]Institute of Pathology, University of Wuerzburg, Wuerzburg, Germany; [4]Institute of Cancer Sciences, University of Glasgow, and the CRUK Beatson Institute, Glasgow, UK; [5]Institute of Biomedical Research, College of Medical and Dental Sciences, University of Birmingham, Birmingham, UK

* equal contribution

[6]Correspondence to:

Stefan Gaubatz

Phone (+49) 931-31-84138

e-mail:stefan.gaubatz@biozentrum.uni-wuerzburg.de

ABSTRACT

The conserved Myb-MuvB multiprotein complex plays an important role in transcriptional activation of mitotic genes. Myb-MuvB target genes are overexpressed in several different cancer types, and their elevated expression is associated with an advanced tumor state and a poor prognosis. This suggests that Myb-MuvB could contribute to tumorigenesis by mediating overexpression of mitotic genes. However, although Myb-MuvB has been extensively characterized biochemically, the requirement for Myb-MuvB in tumorigenesis *in vivo* has not been investigated. Here we demonstrate that Myb-MuvB is required for tumor formation in a mouse model of lung cancer driven by oncogenic K-RAS. We also identify a requirement for the mitotic kinesin KIF23, a key target gene of Myb-MuvB, in tumorigenesis. RNAi mediated depletion of KIF23 inhibited lung tumor formation *in vivo*, and induced apoptosis in lung cancer cell lines. Our results suggest that inhibition of KIF23 could be a strategy for treatment of lung cancer.

Key words: Myb-MuvB, KIF23, lung cancer mouse model,

INTRODUCTION

Mitotic proteins, such as spindle checkpoint proteins, key mitotic kinases and proteins required for cytokinesis, are frequently expressed at elevated levels in cancer cells. Increased expression of mitotic proteins is probably, at least in part, due to a higher fraction of proliferating cells in tumor tissue. However, many mitotic genes that are expressed at elevated levels in tumors are part of recently published chromosomal instability (CIN) signatures that predict the clinical outcome of various cancer types independent of the cell cycle score.[1-3] Thus elevated expression of some of mitotic genes could play a causal role in tumor initiation or progression due to the abnormal execution of mitosis resulting in defects in chromosome segregation and aneuploidy. Mouse models have confirmed that the overexpression of mitotic proteins such as the spindle checkpoint protein MAD2 or the kinetochore protein HEC1 is sufficient to generate aneuploidy and to induce various tumors,

including lung adenomas.[4,5] Several causes for the overexpression of mitotic genes in cancer cells have been identified. For example, inactivation of the retinoblastoma tumor suppressor protein leads to abnormal expression of MAD2 by E2F transcription factors.[6] Similarly, the c-MYC oncogene activates BUBR1 and MAD2 which in turn provoke a prometaphase delay that underlies the chromosomal missegregation induced by c-MYC.[7]

Another key regulator of mitotic genes is the Myb-MuvB complex (reviewed in ref 8). MuvB is the core of an evolutionary conserved complex that regulates transcription during the cell cycle. Specifically, in quiescent cells MuvB, consisting of LIN9, LIN37, LIN52, LIN54 and RBBP4, associates with the p130 pocket protein and with E2F4 to form DREAM, which represses transcription.[9,10] In contrast, in S phase, the interaction of the MuvB core with p130/E2F4 is lost and MuvB now binds to the B-MYB transcription factor to form the Myb-MuvB complex (also called MMB).[10-12] In late S-phase the transcription factor FoxM1 is also recruited into the complex.[11] In contrast to DREAM, Myb-MuvB and MMB-FoxM1 act as transcriptional activators. Genome wide expression studies and chromatin immunoprecipitation (ChIP) assays revealed that MMB and FoxM1 regulate late cell cycle genes with functions in mitosis and cytokinesis such as PLK1, cyclin B or the kinesin KIF20A and that its inactivation results in mitotic defects.[11-15] Interestingly, at least 10 out of 29 mitotic genes included in the above-mentioned CIN signature of lung, brain and breast tumors are directly regulated by Myb-MuvB and FoxM1. Thus Myb-MuvB could promote tumorigenesis by activating the expression of critical mitotic genes.

The relationship of Myb-MuvB to tumorigenesis is largely unknown and whether Myb-MuvB contributes to tumorigenesis *in vivo* has not directly been tested. Here we used a mouse model of lung cancer driven by oncogenic K-RAS and loss of p53 to investigate the requirement for Myb-MuvB during tumorigenesis *in vivo*. We find that Myb-MuvB is required for lung tumor development and that Myb-MuvB drives the expression of mitotic kinesins in lung cancer cells. Depletion of the mitotic kinesin KIF23, one of several genes regulated by Myb-MuvB, inhibits lung tumorigenesis and induces apoptosis *in vitro* and *in vivo*. Together these data establish a requirement for Myb-MuvB regulated genes for lung tumorigenesis.

RESULTS

Myb-MuvB is required for lung tumor formation in vivo

Little is known about the role of Myb-MuvB in cancer *in vivo*. To investigate whether Myb-MuvB is involved in lung tumorigenesis, we used a well-characterized *in vivo* mouse model of NSCLC driven by oncogenic K-RAS and loss of p53 (ref.16). This mouse model is based on a conditional allele of oncogenic *K-Ras* (*LSL-K-Ras*^{G12D}) and conditional loss of function *p53* alleles (*p53*$^{fl/fl}$) (Fig. 1A). Controlled activation of oncogenic K-RAS^{G12D} and loss of p53 in the lung is achieved by adenoviral or lentiviral Cre-recombinase, leading to the development of atypical adenomatous hyperplasias (AAH), adenomas, adenocarcinomas and invasive adenocarcinomas in the lungs within 13 weeks (Supplementary Figure S1).[16,17] B-MYB expression was induced during this process as demonstrated by immunohistochemistry with an antibody that detects active B-MYB phosphorylated on threonine 487 by Cyclin A/CDK2 (Fig. 1B).[11,18] In contrast, in normal lung, no phospho-B-MYB expression could be detected. In tumors, phospho-B-MYB was expressed at higher levels in advanced stage adenocarcinomas (grade 3 and 4) compared to adenomas (grade 2) and low-grade atypical adenomatous hyperplasias (grade 1) (Fig. 1C, D). B-MYB (phospho-T487) immunohistochemistry in 11 human adenocarcinomas of the lung showed moderate to strong protein expression in all tumors (representative stainings shown in Fig. 1E), suggesting that it might have a role in lung tumorigenesis. Examination of previously published microarray data sets showed that high expression levels of B-MYB or of the Myb-MuvB subunit LIN9 were associated with poor prognosis of lung adenocarcinoma patients (Fig. 1F). Furthermore, B-MYB protein expression was higher in lung cancer cell lines compared to non-transformed control cell lines (Fig. 1G).

To directly address the relevance of these findings for tumor initiation and progression *in vivo*, we crossed *LSL-K-Ras*^{G12D}; *p53*$^{fl/fl}$ mice with mice with conditional loss of function alleles of B-MYB or the MuvB subunit LIN9 (*B-Myb*$^{fl/fl}$ or *Lin9*$^{fl/fl}$) (Fig. 2A).[15,19] Infection with Cre

vectors results in simultaneous activation of K-Ras^{G12D}, deletion of p53 and deletion of either B-Myb or Lin9 (Fig. 1A,2A). *LSL-K-Ras^{G12D}*; *p53$^{fl/fl}$* mice with wildtype alleles of B-Myb and Lin9 served as respective controls. As additional controls, mice that retain one functional allele of B-Myb or Lin9 (*Lin9$^{fl/+}$* and *B-Myb$^{fl/+}$*) after Cre-mediated recombination were used. At 13 weeks after tumor initiation with equal biological titers of Cre-virus, *B-Myb$^{fl/fl}$* and *Lin9$^{fl/fl}$* mice showed significantly smaller tumors than control mice (Fig. 2B-D,F-H). In comparison to control mice, tumors in *B-Myb$^{fl/fl}$* and *Lin9$^{fl/fl}$* mice were also less advanced (Fig. 2E,I). Specifically, the tumors in *B-Myb$^{fl/fl}$* and *Lin9$^{fl/fl}$* mice showed a lower tumor grade. Based on these data we conclude that Myb-MuvB is required for lung cancer driven by oncogenic K-RAS *in vivo*. The relative tumor area in mice that retain one allele of *B-Myb* was comparable to that observed in control animals, suggesting that loss of one allele of *B-Myb* does not influence tumorigenesis. In contrast, relative tumor burden in heterozygous *Lin9$^{fl/fl}$* mice was slightly increased compared to *Lin9$^{+/+}$* mice. Although the difference did not reach statistical significance, this might suggest that Lin9 can behave as an haploinsufficient tumor suppressor and as an oncogene in the same tumor type, similar to what has been observed for KLF4.[20]

Next, to assess the efficiency of Cre-mediated recombination in tumors we determined the status of the *B-Myb* and *Lin9* alleles by genomic PCR. In all tumors from *LSL-K-Ras^{G12D}*; *p53$^{fl/fl}$*; *B-Myb$^{fl/fl}$* mice, a band corresponding to the unrecombined, floxed allele of *B-Myb* was detected, indicating incomplete inactivation of *B-Myb* (Fig. 3A). Similarly, tumors from *LSL-K-Ras^{G12D}*; *p53$^{fl/fl}$*; *Lin9$^{fl/fl}$* mice retained unrecombined alleles of Lin9 (Fig. 3B). To determine the expression of B-MYB in tumors from *LSL-K-Ras^{G12D}; p53$^{fl/fl}$; B-Myb$^{fl/fl}$* mice compared to control mice, we performed immunohistochemistry (Fig. 3C,D). We found lower expression of B-MYB in the majority of tumors from *LSL-K-Ras^{G12D}; p53$^{fl/fl}$; B-Myb$^{fl/fl}$* mice compared to controls (Fig. 3D). However, B-MYB expression was not completely lost in these tumors. LIN9 protein expression could not be investigated due to the lack of a suitable antibody for immunohistochemistry. Taken together, these results suggest that there is a strong selection

against the complete loss of LIN9 or B-MYB in tumors and that only tumors that escape the complete deletion of LIN9 or B-MYB are able to progress. The strong dependency on LIN9 and B-MYB likely explains the difference in tumor formation in *LSL-K-Ras^{G12D};p53$^{fl/fl}$;Lin9$^{fl/fl}$* and *LSL-K-Ras^{G12D};p53$^{fl/fl}$;B-Myb$^{fl/fl}$* mice compared to control mice. Incomplete deletion of tumor-essential genes in this *in vivo* model is consistent with previous reports using conditional Rac1-, CK1α- and JNK-deficient mice.[21-23]

A requirement for Myb-MuvB in lung tumor cells in vitro

To investigate the requirement for MuvB during proliferation of lung cancer cells *in vitro*, we next established primary cell lines from dissected lung adenocarcinomas from *LSL-K-Ras^{G12D};p53$^{fl/fl}$;Lin9$^{fl/fl}$* mice (KPL1 and KPL2) and from control *K-Ras^{G12D};p53$^{fl/fl}$* mice with wildtype alleles of Lin9 (KP1 and KP2). We stably expressed the hormone-inducible CreER^{T2} recombinase in KP and KPL cells. Addition of 4-OHT to KPL cells resulted in deletion of the remaining floxed allele of Lin9 and loss of protein expression, but had no effect on the Lin9 wildtype allele or LIN9 protein expression in KP cells, as expected (Fig. 4A,B). Significantly, deletion of Lin9 strongly impaired the proliferation rate of KPL cells, while the addition of 4-OHT had no effect on the proliferation of control cells (Fig. 4C,D). Microscopic examination showed that treatment with 4-OHT resulted in a high frequency of cellular abnormalities including multipolar mitosis, cells with multilobed nuclei and binucleated cells indicative of cytokinesis failure (Fig. 4E and Supplementary Figure S2). Thus loss of Lin9 in lung adenocarcinoma cells leads to nuclear abnormalities and a strong growth inhibition, providing a mechanistic explanation for the inhibitory effect of Lin9 deletion on lung tumorigenesis *in vivo*.

Mitotic genes are targets of Myb-MuvB in lung cancer cells

Previous microarray and ChIP experiments have identified mitotic genes such as the kinesin KIF23 (MKLP1), NUSAP1 and Survivin (BIRC5) as direct transcriptional targets of Myb-MuvB.[14,15,24] To analyze the regulation of mitotic gene expression by Myb-MuvB in lung

cancer cells and to determine the relationship with p53, we used a cell line derived from mouse lung adenocarcinomas with oncogenic *K-Ras*^{G12D} and a nonfunctional *p53* allele which is blocked by a translational STOP cassette that can be removed by an inducible CreER^{T2} recombinase.[25] The addition of 4-OHT to the cell culture medium activates CreER^{T2} recombinase and results in re-expression of p53 (Fig. 5B). Depletion of B-MYB or LIN9 in KPR8 cells (before p53 restoration) by RNA interference reduced the expression of six mitotic kinesins as well as four other Myb-MuvB genes (CENPF, PLK1, BIRC5 and NUSAP1) with functions in mitosis (Fig. 5A).

Restoration of the p53 allele by addition of 4-OHT induced p53 protein expression and strongly activated p21^{CIP1}, a cyclin-dependent kinase inhibitor and a well-known p53-target gene (Fig. 5C). In contrast, mitotic genes were downregulated after p53-restoration, indicating that the Myb-MuvB-dependent genes are repressed after restoration of p53 (Fig. 5C). p53 restoration induced association of p130 with MuvB while it displaced B-MYB from the MuvB core, indicating that activation of p53 promotes formation of the repressive DREAM complex (Fig. 5D). Consistent with these findings, chromatin immunoprecipitation (ChIP) assays showed that binding of B-MYB to the promoters of NUSAP1 and CENP-F was strongly reduced after p53 restoration while binding of p130 was induced (Fig. 5E). These changes correlate with reduced expression of NUSAP1 and CENP-F after p53-restoration. RNAi mediated depletion of Myb-MuvB subunits LIN9 and B-MYB and ChIP experiments in the human lung adenocarcinoma cell line H23 confirmed that Myb-MuvB is required to drive overexpression of mitotic genes (Supplementary Figure S3). Together these data suggest that Myb-MuvB drives expression of mitotic genes in lung carcinoma cells in the absence of functional p53. Consistent with this notion, immunohistochemistry showed that Nusap1 is expressed in murine lung adenocarcinomas and that its expression correlated with tumor grade (Supplementary Figure S4). Furthermore, there is a high correlation between the expression of B-MYB and the Myb-MuvB target gene Nusap1 in individual lung adenocarcinomas *in vivo* (Fig. 5F)

The Myb-MuvB regulated mitotic kinesin KIF23 is required for proliferation of lung cancer cells and for tumor formation in vivo

Although these observations suggest that Myb-MuvB might be a therapeutic target for the treatment of lung cancer, inhibiting its function with small molecules will be difficult to achieve as no enzymatic activities have been identified in the complex. Mitotic kinesins are targets of Myb-MuvB in lung cancer cells (Fig.5 and Supplementary Figure S3). They have emerged as potential new drug targets given their association with chromosomal instability signatures and the correlation of their expression with poor clinical outcome.[26,27] We therefore next selected the Myb-MuvB regulated mitotic kinesin KIF23 (MKLP1) for a more detailed characterization.[24] KIF23, a kinesin of the kinesin-6 family, is a subunit of the centralspindlin complex that is critical for formation of the central spindle.[28] To assess the therapeutic effect of inhibiting KIF23, we used a multifunctional lentiviral vector to establish several stable lung cancer cell lines that express doxycycline-inducible small hairpin RNAs (shRNAs) directed at KIF23 (Fig. 6A). Because upon addition of doxycycline RFP is co-expressed together with the shRNA, we first measured the expression of RFP after treatment with different concentrations of doxycycline to determine the response in the different cell lines. In absence of doxycycline, the cells were RFP-negative, indicating that the system is tightly regulated (Supplementary Figure S5, S6). Addition of doxycycline for three days resulted in a dose-dependent induction of RFP-fluorescence. After addition of 1 µg/ml doxycycline, more than 90% of cells expressed RFP. Treatment with doxycycline resulted in a dose-dependent knockdown of KIF23 protein in the four cell lines (Fig. 6B). Next we investigated the effect of KIF23 depletion on growth of lung cancer lines by treatment of the stable cell lines with different concentrations of doxycycline and by assaying cell number using crystal violet staining. Proliferation of all four cell lines was inhibited by KIF23 depletion (Fig. 6C, Supplementary Figure S7A). The two cell lines H23 and HOP92 were most sensitive to KIF23 depletion and their growth was strongly inhibited even at low concentrations of doxycycline (Fig. 6C). As determined by FACS, the sub G1 population, indicative of degraded DNA, a hallmark of apoptosis, was also strongly increased in these two cell lines

following KIF23 depletion (Fig. 6D). Microscopic examination demonstrated that depletion of KIF23 increased the number of cancer cells with abnormal nuclei such as binucleated cells, multinucleated cells and giant multinucleated cells (Fig. 6E, Supplementary Figure S7B). In summary, our results indicate that depletion of KIF23 induces mitotic catastrophe as characterized by the formation of giant multinucleated cells followed by apoptotic cell death.

To test whether depletion of KIF23 can inhibit lung tumorigenesis *in vivo*, we used the K-RAS dependent NSCLC mouse model described above. For this purpose we created a bifunctional lentivirus that expresses Cre recombinase and in addition a shRNA to knock down KIF23 (Fig. 7A). The shRNA is identical to the one used in human tumor cells due to conservation of the target sequence. Furthermore the KIF23-specific shRNA resulted in efficient knockdown of the KIF23 mRNA in murine NIH-3T3 cells (Supplementary Figure 7C). *LSL-K-Ras^{G12D};p53$^{fl/fl}$* mice were infected with the bifunctional lentivirus to induce lung adenocarcinomas and simultaneously deplete KIF23. In parallel, *LSL-K-Ras^{G12D};p53$^{fl/fl}$* mice were infected with a lentivirus expressing Cre recombinase and a control-shRNA directed at luciferase. Mice were sacrificed 14 weeks after tumor induction and lung tumors were analyzed histologically. Depletion of KIF23 significantly impaired lung tumor development indicating a requirement for KIF23 in K-RAS-driven NSCLC *in vivo* (Fig. 7B,C,D).

DISCUSSION

Myb-MuvB has been identified in previous studies as a master regulator of mitotic gene expression (for review see ref. 11). Myb-MuvB target genes and B-MYB itself are frequently expressed at elevated levels in tumors and their deregulation is associated with more advanced stages of the disease.[1,2] However, whether Myb-MuvB contributes to cancer *in vivo* has not been analyzed. To address this issue, we have used a mouse model of lung adenocarcinoma induced by oncogenic K-RAS and loss of p53. We find that deletion of B-Myb or of Lin9, a core subunit of MuvB, inhibits tumor formation in this model. Mechanistically, we provide evidence that proliferation of lung cancer cells strongly depends

on Myb-MuvB, which acts to activate mitotic genes in these cells. We also show that transcriptional activation by Myb-MuvB is antagonized by p53, corroborating earlier studies of indirect repression of mitotic genes by p53 through formation of DREAM.[29-31] Induction of p53 results in displacement of B-MYB from Myb-MuvB and in formation of the repressive DREAM-p130 complex. Collectively, this suggests that Myb-MuvB contributes to the upregulation of G2/M phase specific genes in p53-negative cells.

On the basis of our findings one might consider Myb-MuvB as a therapeutic target for the treatment of lung cancer. However, because no enzymes have so far been identified in the Myb-MuvB complex, inhibiting its function with small molecules will be difficult to achieve. A promising new strategy that has recently emerged is degradation of multidomain scaffold proteins by ligand-induced protein degradation using bifunctional ligands.[32] Here one part of the ligand is specific to the target protein while the other part recruits a cellular E3 ligase that mediates proteasomal degradation of the target. However, the complete inhibition of Myb-MuvB might be problematic, given that the deletion of B-Myb or Lin9 in mice is known to result in lethality.[15,33] Limited inhibition of Myb-MuvB might provide a therapeutic window to treat lung adenocarcinomas. An alternative approach would be to target the downstream targets of Myb-MuvB such as the mitotic kinesin KIF23, which was investigated in this study.

Kinesins are ATP-dependent motor proteins that regulate the dynamic properties of microtubules.[26,34] Of the 45 kinesins in the human genome, at least 16 have been implicated in coordinating mitosis and cytokinesis. They are responsible for the formation and function of the mitotic spindle, chromosome segregation and cytokinesis. Due to their specialized functions in mitosis, mitotic kinesin inhibition might produce fewer side effects compared to microtubule targeting agents currently used in the clinic.

KIF23 belongs to the kinesin-6 family, whose members have non-redundant roles in cytokinesis.[26,35] Expression of KIF23 has been shown to be upregulated in glioma and non-small cell lung cancer compared to normal tissues.[36,37] In addition, KIF23 is associated with a signature of 100 genes whose elevated expression was associated with chromosomal instability and a poor prognosis across 6 different cancer types including breast cancer and

colon cancer.[2] It is possible that the overexpression of KIF23 leads to defects in chromosome segregation, thereby contributing to chromosomal instability (CIN) and aneuploidy, which is tightly associated with tumorigenesis.[38] Although these observations suggest that KIF23 plays a role in tumorigenesis, it has not yet been investigated whether it is required for tumor formation *in vivo*. Here we demonstrate that depletion of KIF23 inhibited lung tumor formation *in vivo*, similar to what is seen with deletion of Myb-MuvB. *In vitro*, the depletion of KIF23 in lung cancer cell lines showed strong anti-proliferative activity, which was accompanied by apoptosis in a subset of cell lines. Cell death in response to KIF23 downregulation could contribute to the reduction in tumor size *in vivo*. Downregulation of KIF23 can inhibit proliferation of glioma cells, suggesting that KIF23 may be therapeutic target for additional tumor types in addition to lung cancer.[37] In future work it will be important to assess the therapeutic potential of inhibiting KIF23 in already established tumors and to asses the toxicities for non-transformed cells.

MATERIALS AND METHODS

Mice

All animals were maintained on a C57BL/6 background. *LSL-K-RAS^{G12D}*, conditional *p53*, conditional *B-Myb* and conditional *Lin9* knockout mice have been described.[39,15,19,40] *LSL-K-RAS^{G12D}* and conditional *p53* mice were obtained from the NCI Mouse Repository, Bethesda, Maryland. Tumors were initiated in 6 to 9 weeks old male and female mice by nasal instillation of calcium phosphate precipitated adenovirus-Cre (Gene Transfer Vector Core, University of Iowa; 10^5 PFU per mouse) or by intratracheal infection of mice with a lentiviral vector expressing Cre-recombinase (10^6 lentiviruses per mouse) as described previously.[17,41] Sample size was based on comparable studies in the literature. To deliver the virus, mice were anesthetized with Ketamin/Xylazin. For infection with the Cre-shLuc (control) or Cre-shKIF23 lentivirus, *LSL-K-RAS^{G12D};p53$^{fl/fl}$ mice* were randomly allocated to 2 groups. All

animal experiments were carried out according to protocols that were approved by an institutional committee (Tierschutzkommission der Regierung von Unterfranken).

Genotyping of mice, primary tumors and cell lines

The status of the *K-Ras*, *B-Myb* and *Lin9* alleles in tumors and tumor cell lines was analyzed by PCR with previously described primers.[15,19,39] To determine the recombination of *Lin9* and *B-Myb* in primary tumors, genomic DNA was isolated by scraping the tumor material with forceps into 1 ml pure Xylene. Samples were centrifuged for 5 minutes at full speed in a tabletop centrifuge at RT and washed twice with 1 ml absolute ethanol. Genomic DNA from the obtained pellet was further processed and genotyped.

Lentivirus production and titer determination

Lentviruses were produced as described previously.[42] To determine the biological lentiviral titer, we first generated a Cre-reporter cell line by stably transfecting NIH-3T3 cells with the GFP-reporter plasmid pZ/EG.[43] For titer determination, the Z/EG reporter cell line (which expresses GFP after Cre-mediated recombination) was infected with serially diluted lentivirus. The fraction of GFP-positive cells was determined by FACS.

Cell culture

H23, H460, HOP62, HOP92, H226, H522, H358, H441 and A549 cells were cultured in RPMI containing 10% FCS (Invitrogen). BJ, WI38, and KPR8 cells were cultured in DMEM (Invitrogen) containing 10% FCS (Invitrogen). Human cell lines have been authenticated by the multiplex human cell line authentication test (MCA, Multiplexion). To re-activate p53 in KPR8 cells, cells were treated with 500 nM 4-hydroxytamoxifen (Sigma) for the indicated time.[25]

Histopathology and immunohistochemistry

Mouse lung tissues were fixed in 4% paraformaldehyde in PBS, embedded in paraffin and sectioned. Sections were deparaffinised, rehydrated and stained with hematoxylin and eosin or processed for immunohistochemistry staining. Tumor grading was performed in a blinded manner in accordance to the literature.[17] For immunohistochemistry, sections were incubated for 15 minutes with 3% H_2O_2 to quench endogenous peroxidase. Antigen retrieval was performed in 10 mM sodium citrate buffer (pH 6.0) by boiling in a microwave for 15 minutes. Slides were blocked with 3% BSA in PBS and incubated with relevant primary antibodies overnight at 4°C. Secondary antibody was applied to sections at 1:200, incubated for 60 min at RT and developed in diaminobenzidine (DAB). Human adenocarcinomas of the lung were stained immunohistochemically using the anti-B-MYB (phospho T487) antibody (clone EPR2204Y, rabbit monoclonal, 1:100 dilution, Abcam) following antigen retrieval with pressure cooking (citric acid pH 6.0).

Isolation of tumor cell lines

KP and KPL cell lines were derived by enzymatic and mechanical dissociation of individual lung tumors as described previously.[44] Briefly, tumors were dissected under aseptic conditions and minced with sterile razor blades in 2 ml Trypsin/EDTA (0.25%) in a 100 mm cell culture dish. After 30 minutes of trypsinisation at 37°C, the reaction was stopped with 10 ml fresh media. Tissue was broken up by pipetting and the cell suspension was cultured in media supplemented with Mouse FibrOut™ 9 (CHI Scientific). Cells were cultured until confluency was reached, genotyped and stored for further processing.

Antibodies

The following primary antibodies were used: LIN9: ab62329 (Abcam); B-MYB: LX015.1 (kind gift from Roger Watson).[45] p-B-MYB (T487): ab76009 (Abcam). NUSAP1: kind gift from Geert Carmeliet.[46] p130: sc-317 (Santa Cruz Biotechnology). KIF23: sc-22793 (Santa Cruz Biotechnology); p53 (Pab240; sc-99) (Santa Cruz Biotechnology); Tubulin: clone B-5-1-2 (Sigma). Actin: sc-47778 (Santa Cruz).

Immunoprecipitation and immunoblotting

Cells were lysed in TNN [50 mM Tris (pH 7.5), 120 mM NaCl, 5 mM EDTA, 0.5% NP40, 10 mM $Na_4P_2O_7$, 2 mM Na_3VO_4, 100 mM NaF, 10 mg/mL phenylmethylsulfonyl fluoride, protease inhibitors (Sigma)]. Whole cell lysates were immunoprecipitated with antibodies over night at 4 °C, bound to Protein-G-Sepharose for 2 h and washed 5 times with TNN lysis buffer. Proteins were separated by SDS-PAGE, transferred to PVDF membrane and detected by immunoblotting.

Chromatin Immunoprecipitation (ChIP)

Cells were cross-linked with 1% formaldehyde for 10 min at room temperature. The reaction was stopped by adding 125 mM glycine. Cells were lysed for 10 min in lysis buffer [5 mM PIPES (pH 8.0), 85 mM KCl, 0.5% NP40, protease inhibitors (Sigma)]. Nuclei were lysed in nuclei lysis buffer [50 mM Tris (pH 8.1), 10 mM EDTA, 1% SDS, protease inhibitors (Sigma)]. Chromatin was sonicated to an approximate length of 250 to 500 bp, diluted 1:10 with dilution buffer [0.01% SDS, 1.1% Triton, 1.2 mM EDTA, 16.7 mM Tris (pH 8.2), 167 mM NaCl, protease inhibitors (Sigma)] and used for immunoprecipitation overnight. Immmunoprecipitates were collected with protein G–dynabeads (Life Technologies) for 1 h (blocked with 1 mg/mL BSA and 0.3 mg/ml ssDNA). Beads were washed seven times with LiCl washing buffer [0.25 mM LiCl, 0.5% NP40, 0.5% sodium deoxycholate, 1 mM EDTA, 10 mM Tris (pH 8.0), protease inhibitors (Sigma)] and eluted with elution buffer [50 mM Tris (pH 8.0), 1% SDS, 10 mM EDTA]. The cross-link was reversed overnight with 0.2 mM NaCl at 65°C. After proteinase K incubation for 2 h at 55°C, chromatin was purified using Qiagen DNA purification spin columns and eluted in 50 µl. Chromatin (1 µl) was used as template for quantitative real-time PCR.

RNAi

The siRNAs targeting human and murine LIN9 and B-MYB have been described before.[12-14,29] Double stranded RNA was purchased from MWG. siRNAs were transfected in a final concentration of 50 nM using Lipofectamine 2000 (Invitrogen) according to the manufacturer's protocol.

For inducible expression of a KIF23 shRNA in lung cancer cells, the lentiviral pINDUCER10 vector was first modified by replacing the puromycin resistance gene for a blasticidin resistance gene.[47] Next, a mir30 based shRNA specific for KIF23 was cloned into the vector. The targeting sequence for KIF23 is: 5' CCCAGAGTTTGCAGATATGATA 3'. Lung cancer cell lines stably expressing KIF23 specific shRNA were generated by lentiviral infection and selection with blasticidin.

RNA isolation, reverse transcription and quantitative real-time PCR

Total RNA was isolated with Total RNA Isolation Reagent (Thermo Scientific). 1 µg RNA was transcribed using 125 units MMuLv (Thermo Scientific). Quantitative real–time PCR reagents were from Thermo Scientific and real-time PCR was performed using the Mx3000 (Stratagene) detection system. Expression differences were calculated as described before.[10]

Statistical analysis

Statistical analyses were performed using Prism 5 (GraphPad Software). Statistical significance was determined using Student's t test. P values <0.05 were considered statistically significant. Survival analyses for human lung adenocarcinoma patients were computed using an online tool (http://kmplot.com). Log-rank was automatically computed.[48]

CONFLICT OF INTEREST

The authors declare that there is no conflict of interest.

ACKNOWLEDGEMENTS

We thank Tyler Jacks, Anton Berns, Roger Watson, Geert Carmeliet, Thorsten Stiewe and Andras Nagy for reagents and Sabine Roth and Susi Spahr for excellent technical help. We thank all members of the laboratory for their suggestions and critical reading of the manuscript. This work was supported by grants from the Deutsche Krebshilfe (110928), Sander Stiftung (2015.038.1) and DFG (GA 575/5-2) towards SG.

REFERENCES

1 Carter SL, Eklund AC, Kohane IS, Harris LN, Szallasi Z. A signature of chromosomal instability inferred from gene expression profiles predicts clinical outcome in multiple human cancers. *Nat Genet* 2006; **38**: 1043–1048.

2 Cheng W-Y, Ou Yang T-H, Anastassiou D. Biomolecular events in cancer revealed by attractor metagenes. *PLoS Comput Biol* 2013; **9**: e1002920.

3 Chibon F, Lagarde P, Salas S, Pérot G, Brouste V, Tirode F *et al.* Validated prediction of clinical outcome in sarcomas and multiple types of cancer on the basis of a gene expression signature related to genome complexity. *Nat Med* 2010; **16**: 781–787.

4 Sotillo R, Hernando E, Díaz-Rodríguez E, Teruya-Feldstein J, Cordón-Cardo C, Lowe SW *et al.* Mad2 overexpression promotes aneuploidy and tumorigenesis in mice. *Cancer Cell* 2007; **11**: 9–23.

5 Díaz-Rodríguez E, Sotillo R, Schvartzman J-M, Benezra R. Hec1 overexpression hyperactivates the mitotic checkpoint and induces tumor formation in vivo. *Proc Natl Acad Sci USA* 2008; **105**: 16719–16724.

6 Hernando E, Nahlé Z, Juan G, Díaz-Rodríguez E, Alaminos M, Hemann M *et al.* Rb inactivation promotes genomic instability by uncoupling cell cycle progression from mitotic control. *Nature* 2004; **430**: 797–802.

7 Menssen A, Epanchintsev A, Lodygin D, Rezaei N, Jung P, Verdoodt B *et al.* c-MYC delays prometaphase by direct transactivation of MAD2 and BubR1: identification of mechanisms underlying c-MYC-induced DNA damage and chromosomal instability. *Cell Cycle* 2007; **6**: 339–352.

8 Sadasivam S, DeCaprio JA. The DREAM complex: master coordinator of cell cycle-dependent gene expression. *Nat Rev Cancer* 2013; **13**:585-595

9 Litovchick L, Sadasivam S, Florens L, Zhu X, Swanson SK, Velmurugan S *et al.* Evolutionarily conserved multisubunit RBL2/p130 and E2F4 protein complex represses human cell cycle-dependent genes in quiescence. *Mol Cell* 2007; **26**: 539–551.

10 Schmit F, Korenjak M, Mannefeld M, Schmitt K, Franke C, Eyss von B *et al.* LINC, a human complex that is related to pRB-containing complexes in invertebrates regulates the expression of G2/M genes. *Cell Cycle* 2007; **6**: 1903–1913.

11 Sadasivam S, Duan S, DeCaprio JA. The MuvB complex sequentially recruits B-Myb and FoxM1 to promote mitotic gene expression. *Genes Dev* 2012; **26**: 474–489.

12 Osterloh L, Eyss von B, Schmit F, Rein L, Hübner D, Samans B *et al.* The human synMuv-like protein LIN-9 is required for transcription of G2/M genes and for entry into mitosis. *EMBO J* 2007; **26**: 144–157.

13 Knight AS, Notaridou M, Watson RJ. A Lin-9 complex is recruited by B-Myb to activate transcription of G2/M genes in undifferentiated embryonal carcinoma cells. *Oncogene* 2009; **28**: 1737–1747.

14 Esterlechner J, Reichert N, Iltzsche F, Krause M, Finkernagel F, Gaubatz S. LIN9, a Subunit of the DREAM Complex, Regulates Mitotic Gene Expression and Proliferation of Embryonic Stem Cells. *PLoS ONE* 2013; **8**: e62882.

15 Reichert N, Wurster S, Ulrich T, Schmitt K, Hauser S, Probst L *et al.* Lin9, a subunit of the mammalian DREAM complex, is essential for embryonic development, for survival of adult mice, and for tumor suppression. *Mol Cell Biol* 2010; **30**: 2896–2908.

16 Jackson EL, Olive KP, Tuveson DA, Bronson R, Crowley D, Brown M *et al.* The differential effects of mutant p53 alleles on advanced murine lung cancer. *Cancer Res* 2005; **65**: 10280–10288.

17 DuPage M, Dooley AL, Jacks T. Conditional mouse lung cancer models using adenoviral or lentiviral delivery of Cre recombinase. *Nat Protoc* 2009; **4**: 1064–1072.

18 Saville MK, Watson RJ. The cell-cycle regulated transcription factor B-Myb is phosphorylated by cyclin A/Cdk2 at sites that enhance its transactivation properties. *Oncogene* 1998; **17**: 2679–2689.

19 García P, Berlanga O, Watson R, Frampton J. Generation of a conditional allele of the B-myb gene. *Genesis* 2005; **43**: 189–195.

20 Tetreault M-P, Yang Y, Katz JP. Krüppel-like factors in cancer. *Nat Rev Cancer* 2013; **13**: 701–713.

21 Kissil JL, Walmsley MJ, Hanlon L, Haigis KM, Bender Kim CF, Sweet-Cordero A *et al.* Requirement for Rac1 in a K-ras induced lung cancer in the mouse. *Cancer Res* 2007; **67**: 8089–8094.

22 Cellurale C, Sabio G, Kennedy NJ, Das M, Barlow M, Sandy P *et al.* Requirement of c-Jun NH(2)-terminal kinase for Ras-initiated tumor formation. *Mol Cell Biol* 2011; **31**: 1565–1576.

23 Bowman BM, Sebolt KA, Hoff BA, Boes JL, Daniels DL, Heist KA *et al.* Phosphorylation of FADD by the kinase CK1α promotes KRASG12D-induced lung cancer. *Science signaling* 2015; **8**: ra9.

24 Fischer M, Grundke I, Sohr S, Quaas M, Hoffmann S, Knörck A *et al.* p53 and Cell Cycle Dependent Transcription of kinesin family member 23 (KIF23) Is Controlled Via a CHR Promoter Element Bound by DREAM and MMB Complexes. *PLoS ONE* 2013; **8**: e63187.

25 Feldser DM, Kostova KK, Winslow MM, Taylor SE, Cashman C, Whittaker CA *et al.* Stage-specific sensitivity to p53 restoration during lung cancer progression. *Nature* 2010; **468**: 572–575.

26 Rath O, Kozielski F. Kinesins and cancer. *Nat Rev Cancer* 2012; **12**: 527–539.

27 Huszar D, Theoclitou M-E, Skolnik J, Herbst R. Kinesin motor proteins as targets for cancer therapy. *Cancer Metastasis Rev* 2009; **28**: 197–208.

28 White EA, Glotzer M. Centralspindlin: at the heart of cytokinesis. *Cytoskeleton (Hoboken)* 2012; **69**: 882–892.

29 Mannefeld M, Klassen E, Gaubatz S. B-MYB is required for recovery from the DNA damage-induced G2 checkpoint in p53 mutant cells. *Cancer Res* 2009; **69**: 4073–4080.

30 Quaas M, Müller GA, Engeland K. p53 can repress transcription of cell cycle genes through a p21(WAF1/CIP1)-dependent switch from MMB to DREAM protein complex

binding at CHR promoter elements. *Cell Cycle* 2012; **11**: 4661–4672.

31 Fischer M, Quaas M, Steiner L, Engeland K. The p53-p21-DREAM-CDE/CHR pathway regulates G2/M cell cycle genes. *Nucleic Acids Res* 2015. **44**:164-174

32 Winter GE, Buckley DL, Paulk J, Roberts JM, Souza A, Dhe-Paganon S *et al.* DRUG DEVELOPMENT. Phthalimide conjugation as a strategy for in vivo target protein degradation. *Science* 2015; **348**: 1376–1381.

33 Tanaka Y, Patestos NP, Maekawa T, Ishii S. B-myb is required for inner cell mass formation at an early stage of development. *J Biol Chem* 1999; **274**: 28067–28070.

34 Hirokawa N, Noda Y, Tanaka Y, Niwa S. Kinesin superfamily motor proteins and intracellular transport. *Nat Rev Mol Cell Biol* 2009; **10**: 682–696.

35 Glotzer M. The 3Ms of central spindle assembly: microtubules, motors and MAPs. *Nat Rev Mol Cell Biol* 2009; **10**: 9–20.

36 Välk K, Vooder T, Kolde R, Reintam M-A, Petzold C, Vilo J *et al.* Gene expression profiles of non-small cell lung cancer: survival prediction and new biomarkers. *Oncology* 2010; **79**: 283–292.

37 Takahashi S, Fusaki N, Ohta S, Iwahori Y, Iizuka Y, Inagawa K *et al.* Downregulation of KIF23 suppresses glioma proliferation. *J Neurooncol* 2012; **106**: 519–529.

38 Bakhoum SF, Compton DA. Chromosomal instability and cancer: a complex relationship with therapeutic potential. *J Clin Invest* 2012; **122**: 1138–1143.

39 Jackson EL, Willis N, Mercer K, Bronson RT, Crowley D, Montoya R *et al.* Analysis of lung tumor initiation and progression using conditional expression of oncogenic K-ras. *Genes Dev* 2001; **15**: 3243–3248.

40 Marino S, Vooijs M, van der Gulden H, Jonkers J, Berns A. Induction of medulloblastomas in p53-null mutant mice by somatic inactivation of Rb in the external granular layer cells of the cerebellum. *Genes Dev* 2000; **14**: 994–1004.

41 Murphy DJ, Junttila MR, Pouyet L, Karnezis A, Shchors K, Bui DA *et al.* Distinct thresholds govern Myc's biological output in vivo. *Cancer Cell* 2008; **14**: 447–457.

42 Tiscornia G, Singer O, Verma IM. Production and purification of lentiviral vectors. *Nat Protoc* 2006; **1**: 241–245.

43 Novak A, Guo C, Yang W, Nagy A, Lobe CG. Z/EG, a double reporter mouse line that expresses enhanced green fluorescent protein upon Cre-mediated excision. *Genesis* 2000; **28**: 147–155.

44 Bassères DS, Ebbs A, Levantini E, Baldwin AS. Requirement of the NF-kappaB subunit p65/RelA for K-Ras-induced lung tumorigenesis. *Cancer Res* 2010; **70**: 3537–3546.

45 Tavner F, Frampton J, Watson RJ. Targeting an E2F site in the mouse genome prevents promoter silencing in quiescent and post-mitotic cells. *Oncogene* 2007; **26**: 2727–2735.

46 Raemaekers T, Ribbeck K, Beaudouin J, Annaert W, Van Camp M, Stockmans I *et al.* NuSAP, a novel microtubule-associated protein involved in mitotic spindle organization. *J Cell Biol* 2003; **162**: 1017–1029.

47 Meerbrey KL, Hu G, Kessler JD, Roarty K, Li MZ, Fang JE *et al.* The pINDUCER lentiviral toolkit for inducible RNA interference in vitro and in vivo. *Proc Natl Acad Sci USA* 2011; **108**: 3665–3670.

48 Győrffy B, Surowiak P, Budczies J, Lánczky A. Online Survival Analysis Software to Assess the Prognostic Value of Biomarkers Using Transcriptomic Data in Non-Small-Cell Lung Cancer. *PLoS ONE* 2013; **8**: e82241.

FIGURE LEGENDS

Figure 1: Expression of the Myb-MuvB subunit B-MYB in lung adenocarcimomas. A) Cre-mediated mouse lung cancer model. Infection of *LSL-K-Ras^{G12D};p53$^{fl/fl}$* mice with Cre-expressing Ade-Cre or Lenti-Cre vectors initiates lung tumorigenesis by activation of oncogenic K-RAS^{G12D} and loss of p53 (p53$^{\Delta/\Delta}$). B) Immunohistochemistry staining of p-B-MYB (phospho T487) in lung tumors and adjacent normal lung tissue from *LSL-Kras^{G12D};p53$^{fl/fl}$* mice 13 weeks after tumor initiation. Bar: 50 µm. C) Expression of p-B-MYB (phospho T487) in grade 1 and grade 3 murine *K-Ras^{G12};p53$^{\Delta/\Delta}$* lung tumors as determined by immunohistochemistry. Left: Magnification 5 x. Bar: 150 µm; Right: Magnification: 20 x. Bar: 50 µm D) Quantification of p-B-MYB (phospho T487) and expression in murine lung tumors from grade 1 (atypical adenomous hyperplasia; AAH) to grade 4 invasive adenocarcinoma (see Supplementary Figure S1). E) Expression of p-B-MYB (phospho T487) in human lung adenocarcinoma was determined by immunohistochemistry. Magnification: 100 x (left), 200 x (middle), 400 x (right). F) Kaplan-Meier curves correlating lung adenocarcinoma patients' survival with B-MYB and LIN9 expression. G) B-MYB expression in a panel of human lung cancer cell lines and two control cell lines (BJ and WI38) was analyzed by immunoblotting. Actin was used as a loading control.

Figure 2: Requirement for B-MYB and LIN9 in a mouse model for lung cancer. A) Scheme of the conditional alleles of *Lin9* and *B-Myb*. B) -E) *LSL-Kras^{G12D};p53$^{fl/fl}$;B-Myb$^{+/+}$* (n=14); *Kras^{G12D};p53$^{fl/fl}$;B-Myb$^{fl/+}$* (n=13) and *Kras^{G12D};p53$^{fl/fl}$;B-Myb$^{fl/fl}$* (n=15) mice were infected with Lenti-Cre. Mice were sacrificed 13 weeks after tumor initiation. B) Example lung

images C) Representative histological section stained with haematoxylin and eosin. D) Quantification of tumor area to total lung area. Each symbol represents the analysis of an individual animal. Individual tumor area was obtained by measuring all tumors from 2 sections from each mouse. The black bar indicates the mean. The error bars represent SEM. E) Distribution of tumor grades (n=766 tumors *LSL-Kras^{G12D};p53$^{fl/fl}$;B-Myb$^{+/+}$*; n=652 tumors *LSL-Kras^{G12D};p53$^{fl/fl}$;B-Myb$^{fl/fl}$*). The error bars represent SEM. F)-I) *LSL-Kras^{G12D};p53$^{fl/fl}$;Lin9$^{+/+}$* (n=10); *Kras^{G12D};p53$^{fl/fl}$;Lin9$^{fl/+}$* (n=10) and *Kras^{G12D};p53$^{fl/fl}$;Lin9$^{fl/fl}$* (n=10) mice were infected with Ade-Cre. Mice were sacrificed 13 weeks after tumor initiation. F) Representative lung images G) Representative histological sections stained with haematoxylin and eosin. H) Quantification of tumor area to total lung area. Each symbol represents the analysis of an individual animal. Individual tumor area was obtained by measuring all tumors from 2 sections from each mouse. The black bar indicates the mean. The error bars represent SEM. I) Distribution of tumor grades. (n=708 tumors *LSL-Kras^{G12D};p53$^{fl/fl}$; Lin9$^{+/+}$*; n=647 tumors *LSL-Kras^{G12D};p53$^{fl/fl}$; Lin9$^{fl/fl}$*). The error bars represent SEM. For all panels: *, ** or *** indicates that the differences were statistically significant; *p<0.05; **p<0.001 , *** p<0.0001 ; Student's t-test; two-sided.

Figure 3: Incomplete recombination of B-Myb and Lin9 in lung tumors. A) Genomic PCR of *B-Myb* and *K-Ras* alleles in tumors dissected from *LSL-K-Ras^{G12D};p53$^{fl/fl}$;B-Myb$^{fl/fl}$* mice showing retention of the *B-Myb^{fl}* allele in tumors. fl: un-recombined *B-Myb* allele; ∆fl: recombined *B-Myb* allele. LSL: non-recombined K-*RAS^{G12D}* allele. ∆LSL: recombined *K-Ras^{G12D}* allele *:denotes a background band. B) PCR of *Lin9* and *K-Ras* alleles in tumors dissected from *LSL-K-Ras^{G12D};p53$^{fl/fl}$;Lin9$^{fl/fl}$* mice showing retention of the *Lin9^{fl}* allele. fl: un-recombined Lin9 allele; ∆fl: recombined *Lin9* allele. LSL: non-recombined *K-RAS^{G12D}* allele. ∆LSL: recombined *K-Ras^{G12D}* allele *:denotes a background band. D) Immunohistochemistry staining of lung sections from *LSL-K-Ras^{G12D};p53$^{fl/fl}$;B-Myb$^{fl/fl}$* mice with an anti-p-B-MYB (phospho T487) antibody demonstrates that tumors express B-MYB. Left: 10 x, bar 150 µm; right: 40 x, bar: 50 µm. D) The fraction of tumors expressing low (<10% of cells positive for

B-MYB), medium 1(0-30 % of cells positive for B-MYB) and high (> 30 % of cells positive for B-MYB) levels of phospho-B-MYB in mice of the indicated genotypes was determined by immunohistochemistry.For each genotype, tumors from 4 different mice were analyzed. Number of tumors analyzed: *B-Myb*$^{+/+}$: 233; *B-Myb*$^{fl/+}$: 284; *B-Myb*$^{fl/fl}$: 108.

Figure 4: Adenocarcinoma-derived cell lines are sensitive to the loss of LIN9. A) KP cells (derived from dissected tumors from *LSL-Kras*^{G12D}*;p53*$^{fl/fl}$*;Lin9*$^{+/+}$ mice) and KPL cells (from tumors from *LSL-Kras*^{G12D}*;p53*$^{fl/fl}$*;Lin9*$^{fl/fl}$ mice) were stably transfected with hormone inducible CreER^{T2} recombinase. Treatment with 10 nM 4-OHT results in deletion of the remaining Lin9 allele in KPL cells as determined by genomic PCR. B) LIN9 protein levels in control treated and 4-OHT treated KP and KPL cells were determined by immunoprecipitation followed by immunoblotting. C) and D) Impaired proliferation of lung cancer cells upon deletion of Lin9. KP and KPL cells were seeded at low density and treated with 10 nm 4-OHT or with solvent for 10 days. Cells were fixed and stained with crystal violet. C) Representative example from 3 replicates. D) Growth curves over 10 days. Mean of three independent replicates. Error bars represent standard deviation. **p<0.001 , *** p<0.0001 ; Student's t-test; two-sided. E) Quantification of mitotic defects in KP and KPL cells upon deletion of *Lin9* by treatment with 4-OHT for 3 days. Per condition, 500 to 800 cells were counted. For another time-point and for examples of mitotic defects see Supplementary Figure S2.

Figure 5: Gene regulation by Myb-MuvB in lung cancer cells. A) B-MYB or LIN9 were depleted by RNAi in murine lung cancer KPR8 cells. Expression of the indicated mitotic genes was analyzed by RT-qPCR. Two independent experiments were analyzed in triplicate by qPCR. One representative experiment is shown. B) Restoration of p53 in KPR8 lung adenocarcinoma cells is achieved by addition of 4-OHT, which activates Cre to remove a STOP cassette. C) Mitotic genes are downregulated after p53 re-activation in KPR8 cells as determined by RT-qPCR. p53 protein and the p53-target gene p21 were induced after p53-

restoration, as expected. Two independent experiments were analyzed in triplicate by qPCR. One representative experiment is shown. D) Formation of the repressive DREAM complex and replacement of B-MYB from MuvB after restoration of p53. LIN9 was immunoprecipitated before and after p53-restoration and bound B-MYB and p130 were analyzed by immunoblotting. E) ChIP assay to analyze binding of B-MYB and p130 to the NUSAP1 and CENP-F promoters before and after restoration of p53 by 4-OHT. Binding to the indicated promoters was analyzed by RT-qPCR. Two independent ChIP assay were analyzed in triplicate by qPCR. One representative experiment shown. F) B-MYB and Nusap1 are coexpressed in murine lung adenocarcinomas from K-RAS^{G12D}; p53$^{\Delta/\Delta}$ mice as determined by immunohistochemistry. The table on the right shows the number of tumors with or without B-MYB and NUSAP1 expression. p-value <0.0001, Chi-square, two sided. Bar: 100 µm.

Figure 6: The Muyb-MuvB regulated mitotic kinesin KIF23 is required for proliferation of lung cancer cells. A) Scheme of the pINDUCER vector for doxycycline-inducible expression of the KIF23 shRNA. B) Stable lung cancer cell lines expressing an inducible KI23-specific shRNA were generated. Knockdown of KIF23 after induction of the shRNA with the indicated concentrations of doxycycline was determined by immunoblotting. Actin was used as a loading control. C) Growth of lung cancer cell lines stably expressing the KIF23-specific shRNAs in presence of the indicated concentrations of doxycycline was analyzed over 8 days. Mean of three independent replicates. Error bars represent standard deviation. Significance levels versus control (for reasons of clarity are only indicated for day 8). *p<0.05; **p<0.001 , *** p<0.0001 ; Student's t-test; two-sided. D) The fraction of apoptotic subG1 cells after depletion of KIF23 was determined by FACS. E) Quantification of cells with abnormal nuclei upon depletion of KIF23. Per condition, more than 300 cells were counted. See also Supplementary Figure S7B.

Figure 7: A requirement for KIF23 in lung cancer.

A) Scheme of the bifunctional lentivirus encoding for a mir30 based KIF23-specific shRNA and Cre-recombinase B)-C) *LSL-KRas^{G12D};p53$^{fl/fl}$* mice were infected with a bifunctional lentivirus encoding Cre and a control shRNA (n=7) or with a virus encoding Cre and a shRNA specific for KIF23 (n= 8). B) Representative lung images C) Representative histological section stained with haematoxylin and eosin. D) Quantification of tumor to total lung area. The error bars represent SEM. * indicates that the differences were statistically significant; $p<0.05$; Student's t-test; two-sided.

Figure 1

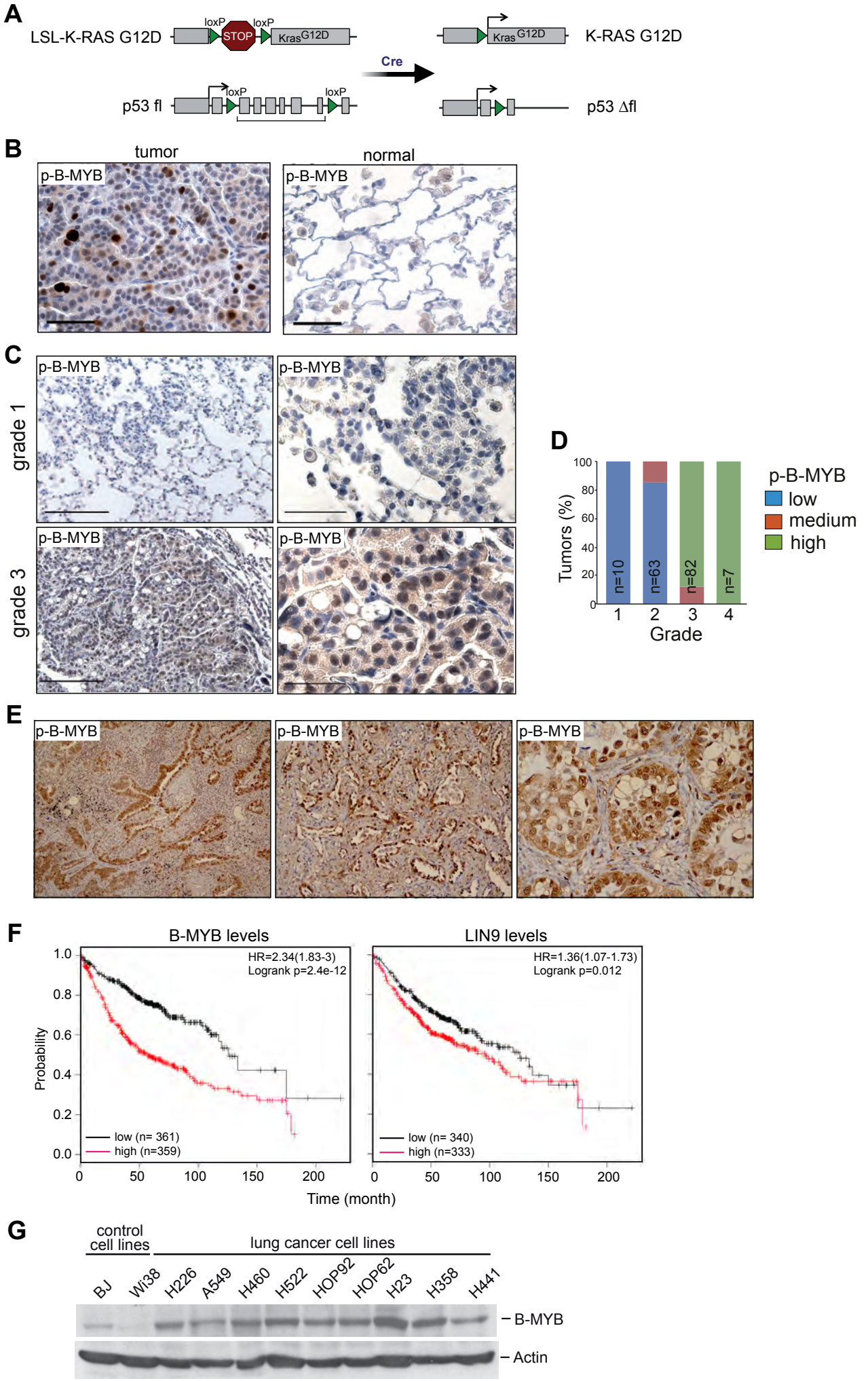
A
LSL-K-RAS G12D
loxP
STOP
loxP
Kras G12D
K-RAS G12D
Cre
p53 fl
loxP
loxP
p53 Δfl
B
tumor
normal
p-B-MYB
C
grade 1
grade 3
p-B-MYB
D
Tumors (%)
100
80
60
40
20
0
n=10
n=63
n=82
n=7
1
2
3
4
Grade
p-B-MYB
low
medium
high
E
p-B-MYB
F
B-MYB levels
HR=2.34(1.83-3)
Logrank p=2.4e-12
low (n= 361)
high (n=359)
LIN9 levels
HR=1.36(1.07-1.73)
Logrank p=0.012
low (n= 340)
high (n=333)
Probability
1.0
0.8
0.6
0.4
0.2
0.0
0
50
100
150
200
Time (month)
G
control cell lines
lung cancer cell lines
BJ
Wi38
H226
A549
H460
H522
HOP92
HOP62
H23
H358
H441
B-MYB
Actin

Figure 2

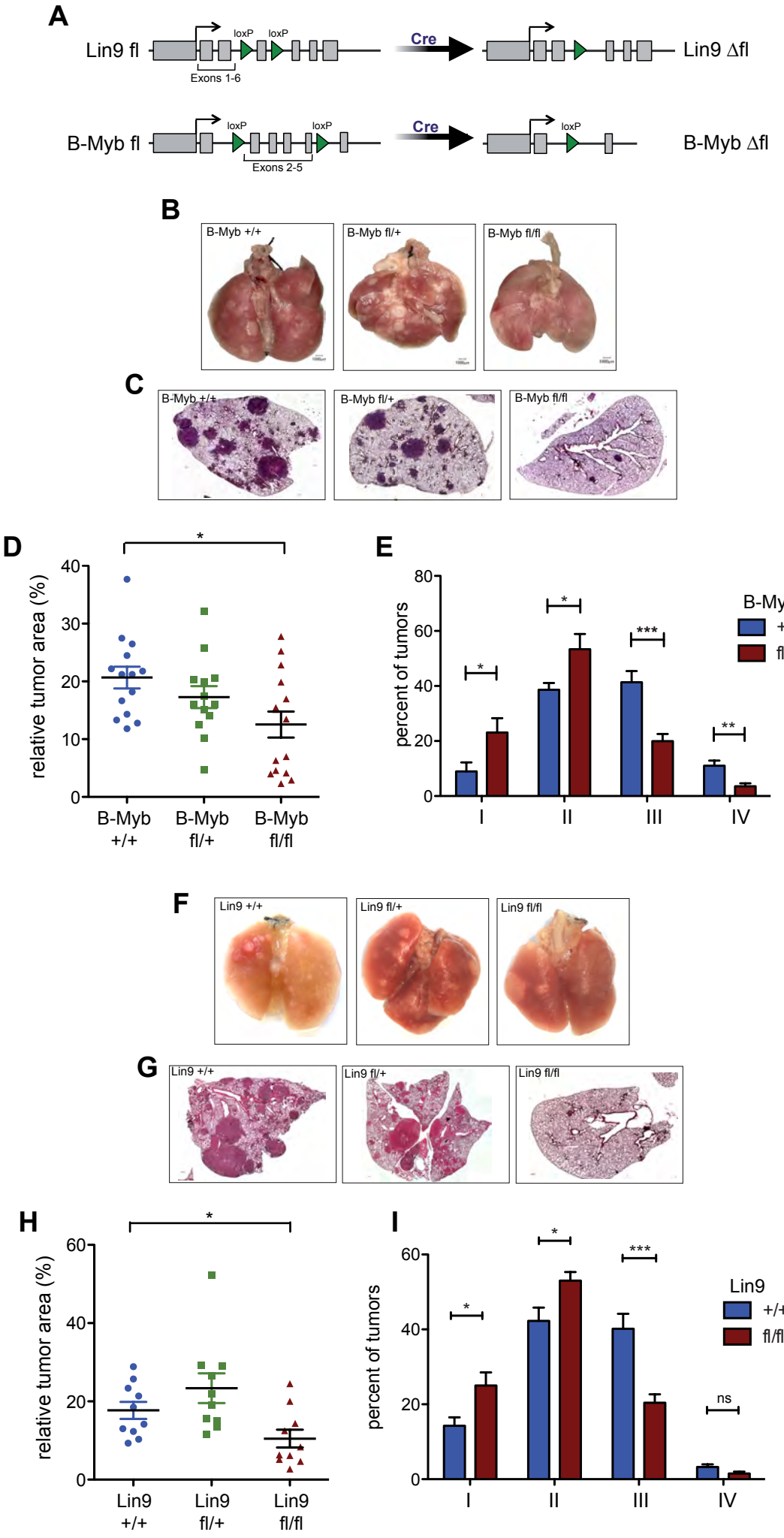
A
Lin9 fl
loxP
loxP
Exons 1-6
Cre
Lin9 Δfl
B-Myb fl
loxP
loxP
Exons 2-5
Cre
loxP
B-Myb Δfl
B
B-Myb +/+
B-Myb fl/+
B-Myb fl/fl
C
B-Myb +/+
B-Myb fl/+
B-Myb fl/fl
D
relative tumor area (%)
40
30
20
10
0
*
B-Myb +/+
B-Myb fl/+
B-Myb fl/fl
E
percent of tumors
80
60
40
20
0
*
*
***
**
I
II
III
IV
B-Myb
+/+
fl/fl
F
Lin9 +/+
Lin9 fl/+
Lin9 fl/fl
G
Lin9 +/+
Lin9 fl/+
Lin9 fl/fl
H
relative tumor area (%)
60
40
20
0
*
Lin9 +/+
Lin9 fl/+
Lin9 fl/fl
I
percent of tumors
60
40
20
0
*
*
***
ns
I
II
III
IV
Lin9
+/+
fl/fl

Figure 3

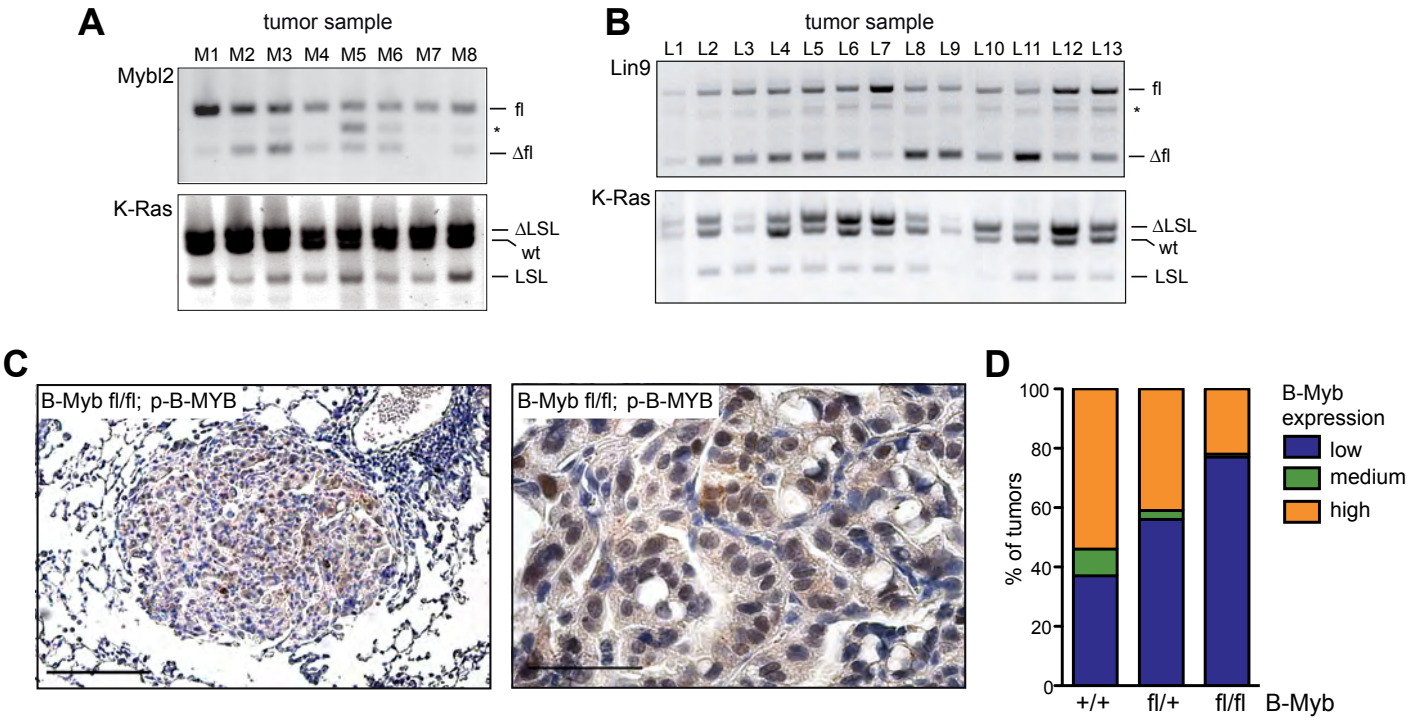
A
tumor sample
M1 M2 M3 M4 M5 M6 M7 M8
Mybl2
fl
*
Δfl
K-Ras
ΔLSL
wt
LSL
B
tumor sample
L1 L2 L3 L4 L5 L6 L7 L8 L9 L10 L11 L12 L13
Lin9
fl
*
Δfl
K-Ras
ΔLSL
wt
LSL
C
B-Myb fl/fl; p-B-MYB
B-Myb fl/fl; p-B-MYB
D
% of tumors
100
80
60
40
20
0
+/+
fl/+
fl/fl
B-Myb
B-Myb expression
low
medium
high

Figure 4

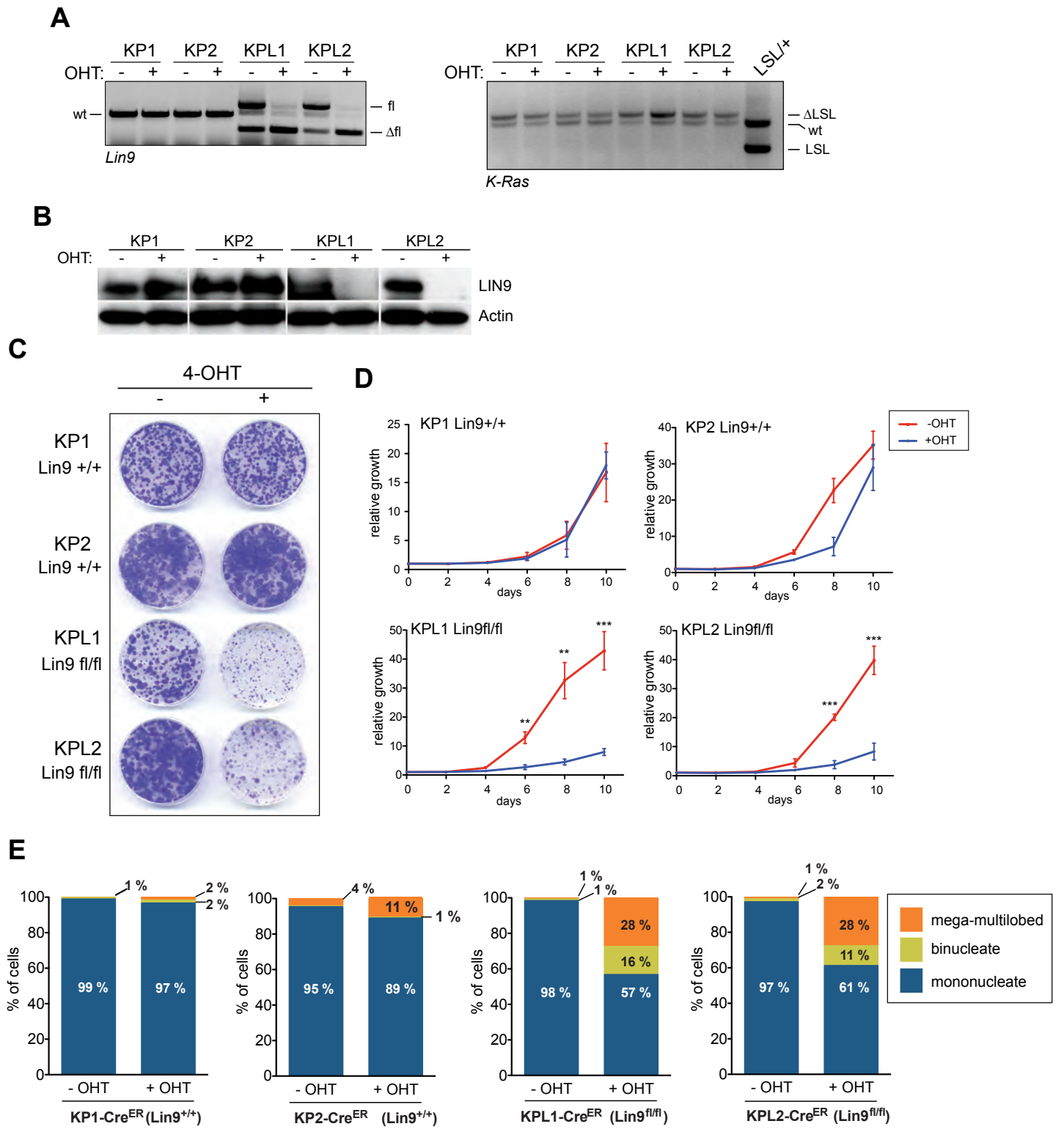
A
KP1
KP2
KPL1
KPL2
OHT:
wt
fl
Δfl
Lin9
LSL/+
ΔLSL
wt
LSL
K-Ras
B
LIN9
Actin
C
4-OHT
KP1
Lin9 +/+
KP2
Lin9 +/+
KPL1
Lin9 fl/fl
KPL2
Lin9 fl/fl
D
KP1 Lin9+/+
KP2 Lin9+/+
KPL1 Lin9fl/fl
KPL2 Lin9fl/fl
relative growth
days
-OHT
+OHT
E
% of cells
99 %
97 %
95 %
89 %
98 %
57 %
28 %
16 %
97 %
61 %
28 %
11 %
mega-multilobed
binucleate
mononucleate
- OHT
+ OHT
KP1-Cre^ER (Lin9^+/+)
KP2-Cre^ER (Lin9^+/+)
KPL1-Cre^ER (Lin9^fl/fl)
KPL2-Cre^ER (Lin9^fl/fl)

Figure 5

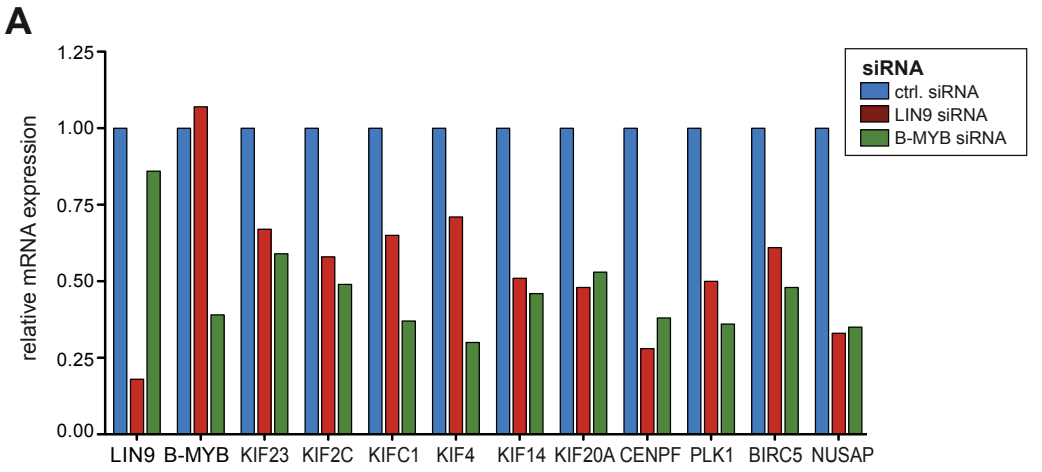

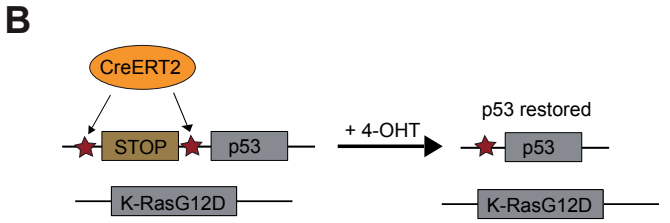

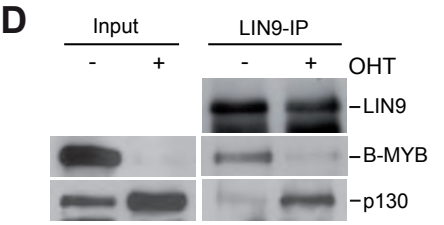

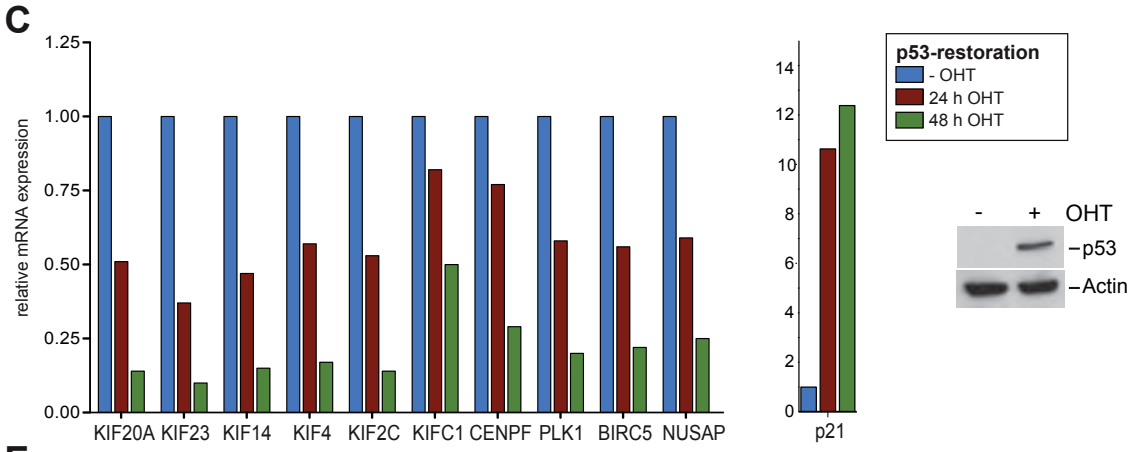

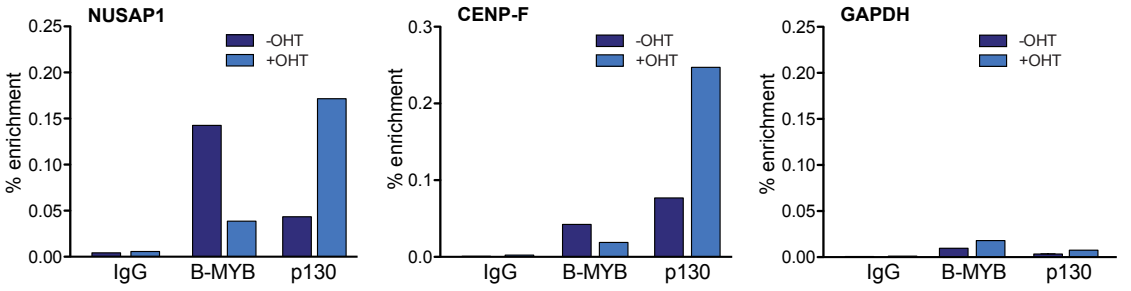

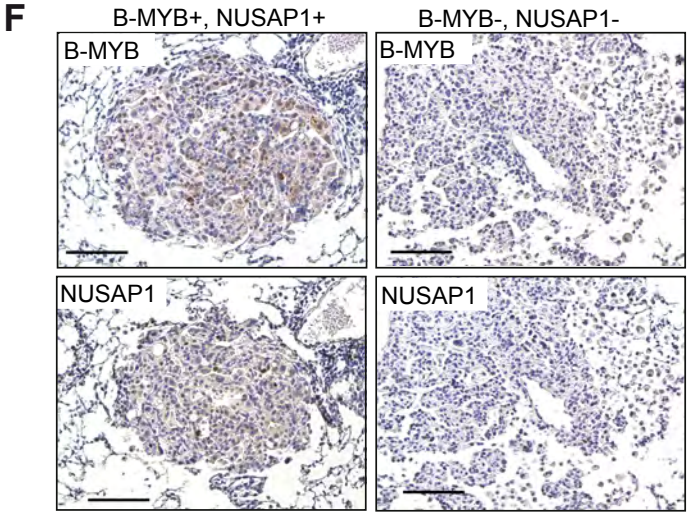

NUSAP1 \ B-MYB	+	-
-	0	14
+	18	3

Figure 6

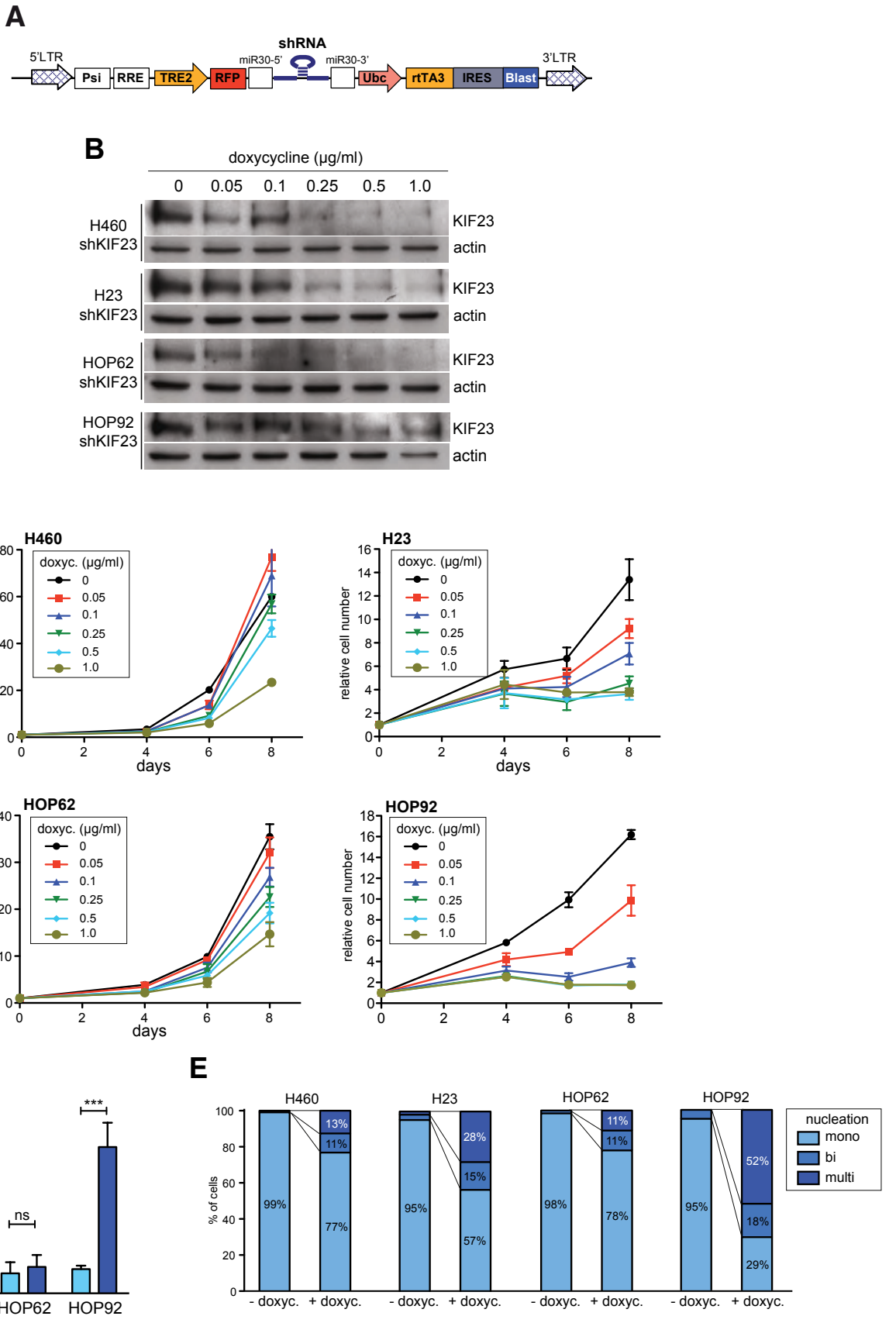
A
shRNA
5'LTR
Psi
RRE
TRE2
RFP
miR30-5'
miR30-3'
Ubc
rtTA3
IRES
Blast
3'LTR
B
doxycycline (μg/ml)
0
0.05
0.1
0.25
0.5
1.0
H460 shKIF23
H23 shKIF23
HOP62 shKIF23
HOP92 shKIF23
KIF23
actin
C
H460
H23
HOP62
HOP92
doxyc. (μg/ml)
relative cell number
days
D
doxycycline
-
+
subG1 (% of cells)
ns
**
***
H460
H23
HOP62
HOP92
E
% of cells
99%
13%
11%
77%
95%
28%
15%
57%
98%
11%
11%
78%
95%
52%
18%
29%
- doxyc.
+ doxyc.
nucleation
mono
bi
multi

Figure 7

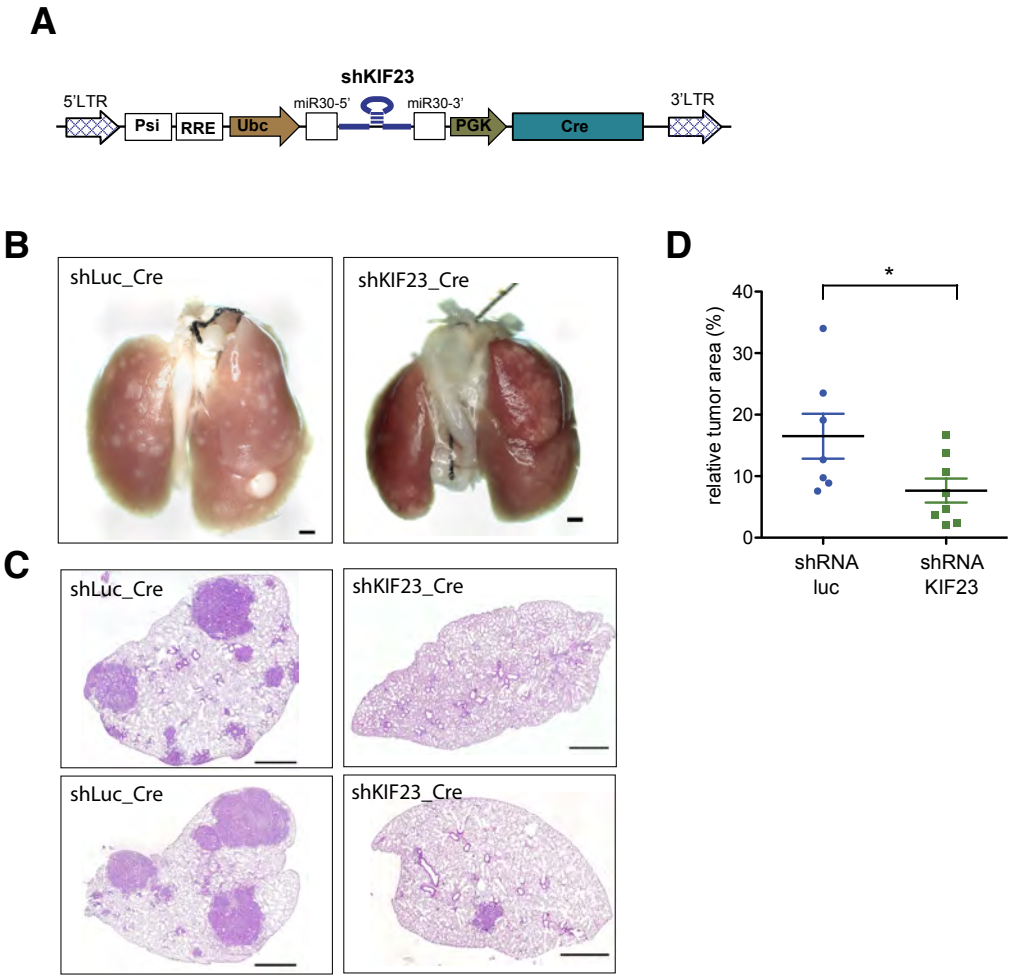
A
shKIF23
5'LTR
Psi
RRE
Ubc
miR30-5'
miR30-3'
PGK
Cre
3'LTR
B
shLuc_Cre
shKIF23_Cre
C
shLuc_Cre
shKIF23_Cre
shLuc_Cre
shKIF23_Cre
D
relative tumor area (%)
40
30
20
10
0
*
shRNA luc
shRNA KIF23

SUPPLEMENTARY FIGURE LEGENDS

Supplementary Figure S1: Tumor grades in Ras^{G12D}; p53$^{\Delta/\Delta}$ lung tumors. Representative histology (H&E) of K-Ras^{G12D}; p53$^{\Delta/\Delta}$ lung tumors 13 weeks after tumor initiation. Grade I: atypical adenomatous hyperplasias (AAH); Grade II: adenomas; Grade III: adenocarcinomas; Grade IV: invasive adenocarcinomas. Size bar: 50 μm.

Supplementary Figure S2: Deletion of Lin9 results in multiple mitotic defects. A) KPL cells were treated with 10nm 4-OHT for 72 hours and cells were fixed and stained with an anti-tubulin antibody (green). DNA was counterstained with Hoechst 33548 (blue). Deletion of Lin9 resulted in binucleated cells, multipolar spindles and cells with large multilobed nuclei. Size bar: 25 μm. B) Quantification of mitotic defects in KP and KPL cells upon deletion of Lin9 by treatment with 4-OHT for 6 days.

Supplementary Figure S3: **Myb-MuvB-dependent expression of mitotic kinesins in the human lung cancer cell line H23.** A) B-MYB or LIN9 were depleted by RNAi in H23 cells. Expression of the indicated kinesins was analyzed by RT-qPCR. B) ChIP assay demonstrating direct binding of B-MYB and LIN9 to the promoters of kinesins but not to the GAPDH promoter in H23 cells. IgG was used as a control.

Supplementary Figure S4: NUSAP1 expression in lung adenocarcinomas. A) Immunohistochemistry staining of NUSAP1 in lung tumors and adjacent normal lung tissue from LSL-Kras^{G12D};p53$^{fl/fl}$ mice 13 weeks after tumor initiation. Bar: 50 μm. B) NUSAP expression correlates with tumor grade. Expression of NUSAP1 in grade 1 and grade 3 murine K-Ras^{G12}; p53$^{\Delta/\Delta}$ lung tumors was determined by immunohistochemistry. Left: Magnification 5 x. Bar: 150 μm; Right: Magnification: 20 x. Bar: 50 μm C) Quantification of NUSAP1 and expression in murine lung tumors relative to tumor grade from grade 1 (see Supplemental Figure S1).

Supplementary Figure S5: Inducible knockdown of KIF23. Lung cancer cell lines stably expressing an inducible KIF23-specific shRNA together with RFP were treated with the indicated concentrations of doxycycline. The expression of RFP was determined by microscopy.

Supplementary Figure S6: Inducible knockdown of KIF23. Lung cancer cell lines stably expressing an inducible KIF23-specific shRNA together with RFP were treated with the indicated concentrations of doxycycline. The expression of RFP was determined by FACS.

Supplementary Figure S7: KIF23 is required for proliferation of lung cancer cell lines. A) The indicated NSCLC cell lines (non-shRNA transfected controls or expressing the KIF23-specific shRNAs) were cultured for 8 days with the indicated concentrations of doxycycline. Colonies were stained with crystal violet. B) Abnormal nuclei after depletion of KIF23. Bar: 25 µm. The indicated cell lines stably expressing the KIF23-specific shRNA were treated with doxycycline for 4 days. Cells were fixed and stained with an anti-tubulin antibody (green). Nuclei were stained with Hoechst 33548 (blue). Bar: 25 µm. C) Knockdown of KIF23 in mouse NIH-3T3 cells by the KIF23-specific shRNA was verified by RT-qPCR.

Supplementary Figure S1

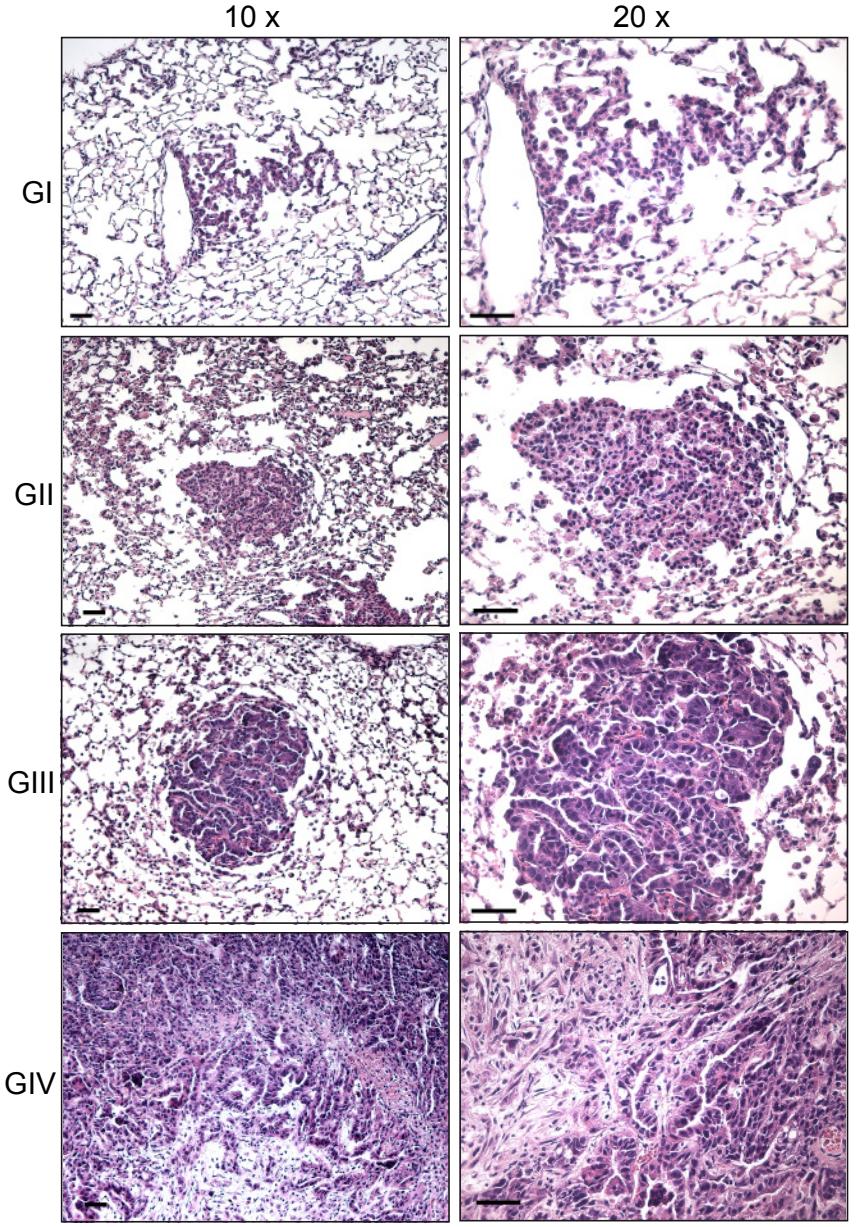

Supplementary Figure S2

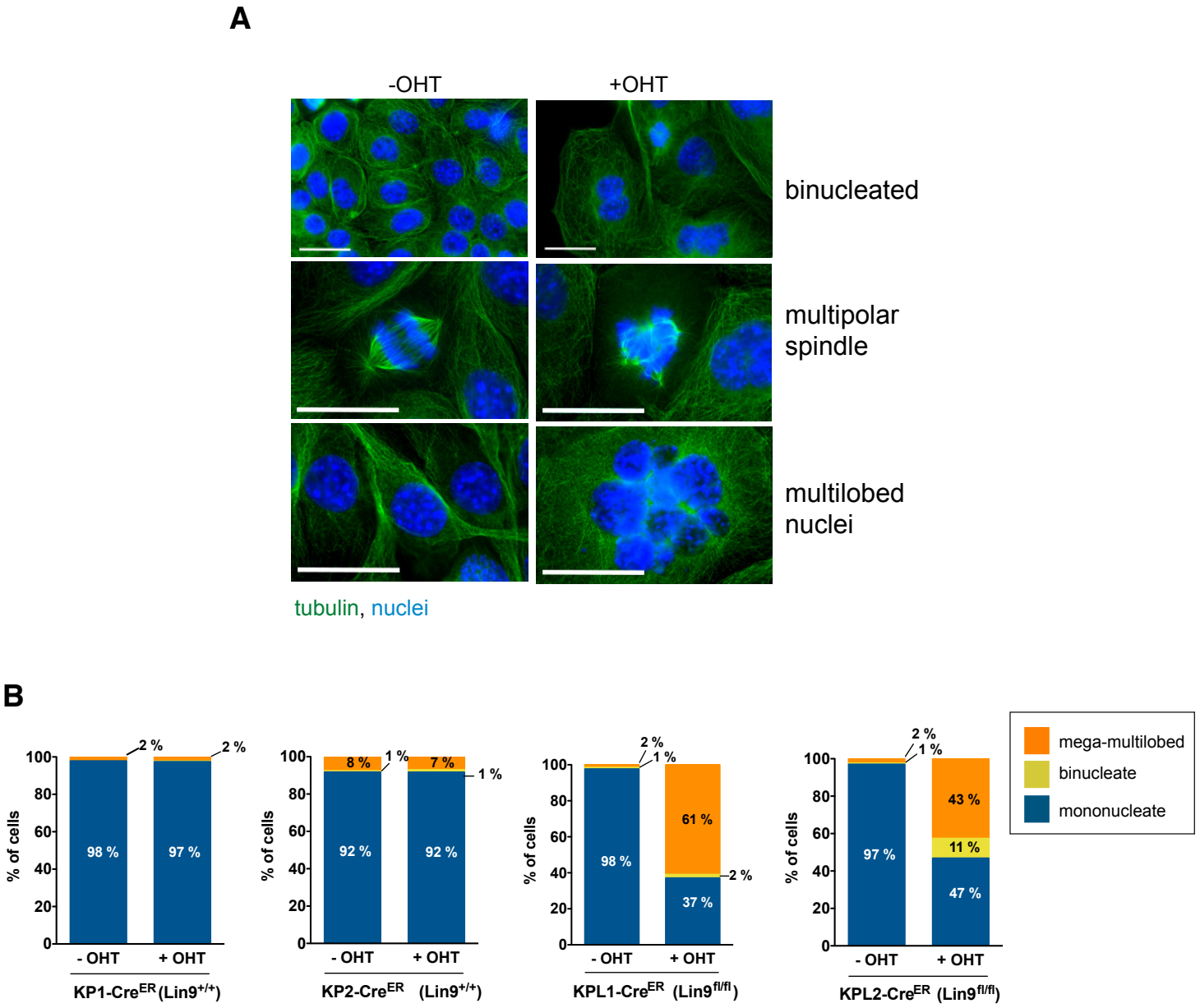

Supplementary Figure S3

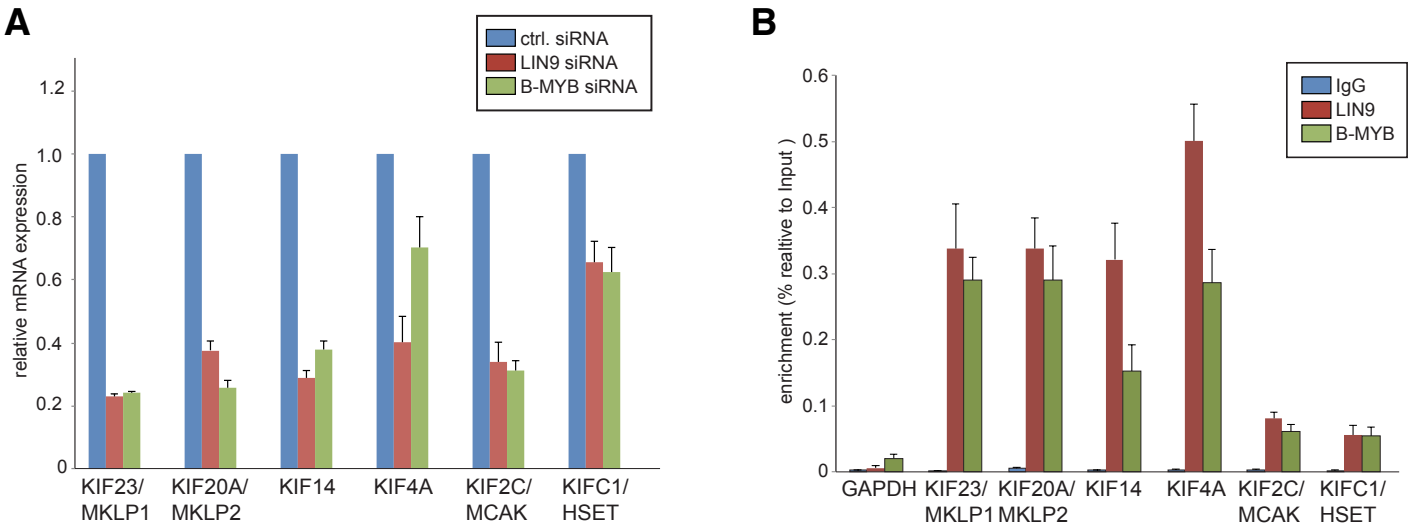

Supplementary Figure S4

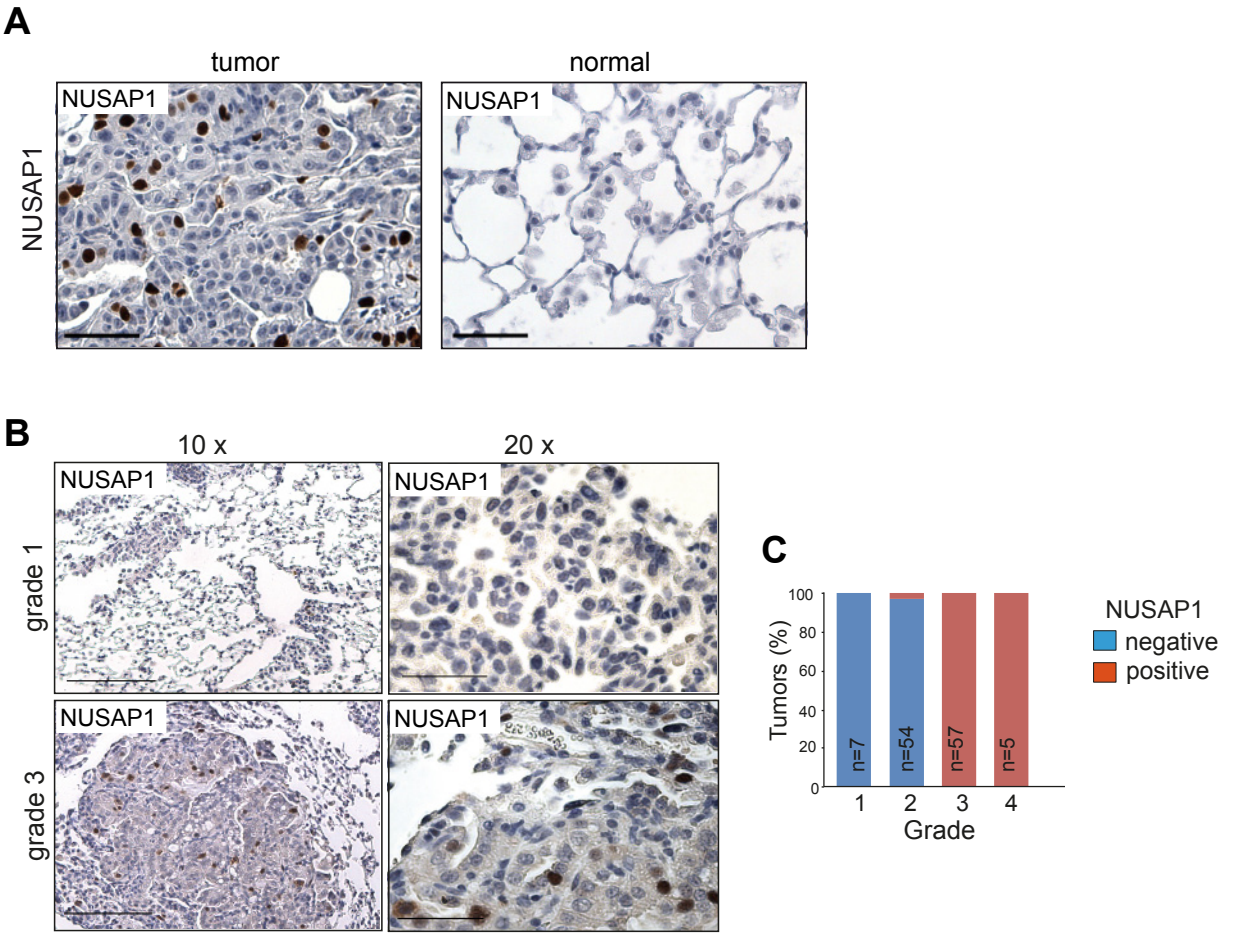

Supplementary Figure S5

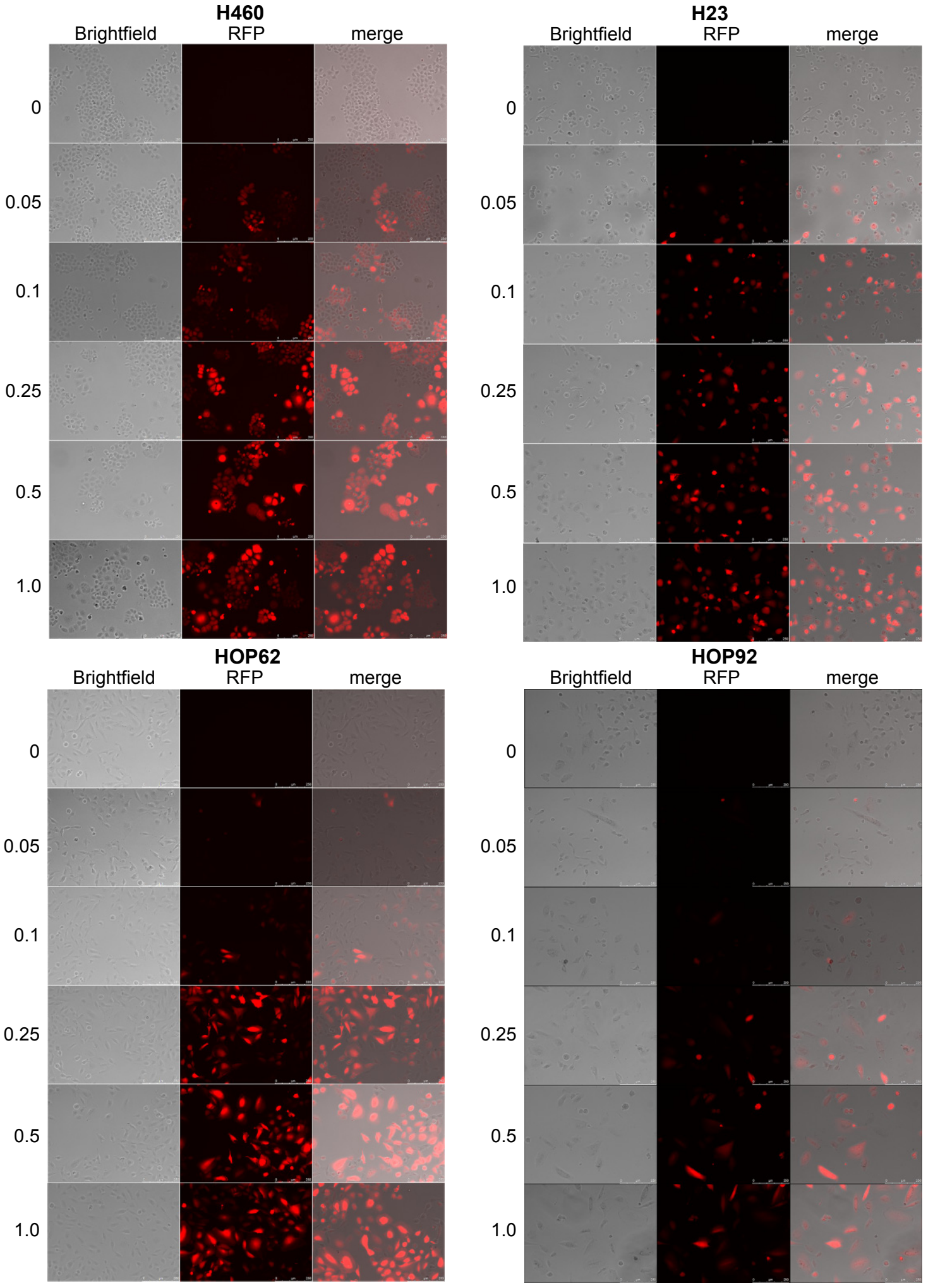

Supplementary Figure S6

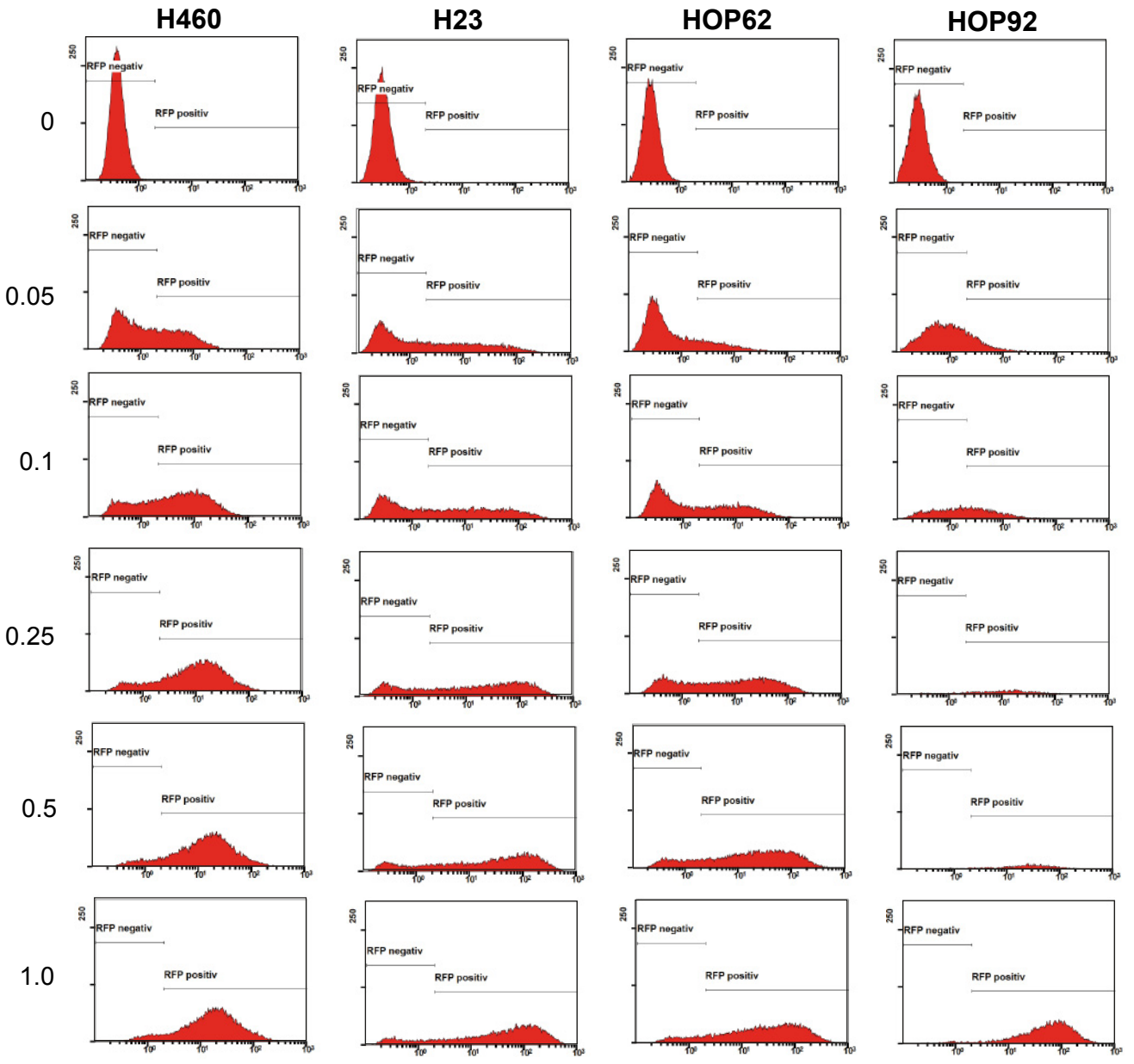

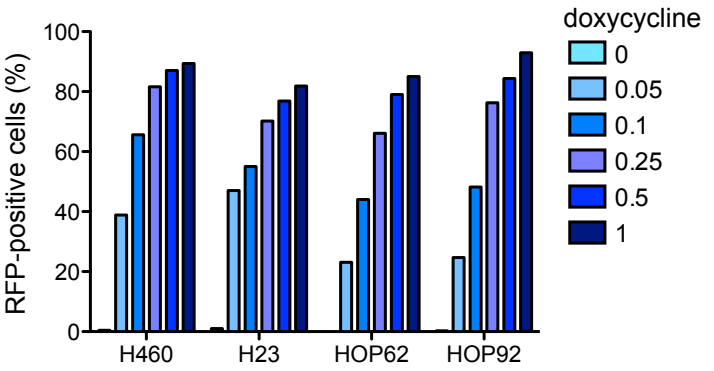

Supplementary Figure S7